

# RSC Advances



This is an *Accepted Manuscript*, which has been through the Royal Society of Chemistry peer review process and has been accepted for publication.

*Accepted Manuscripts* are published online shortly after acceptance, before technical editing, formatting and proof reading. Using this free service, authors can make their results available to the community, in citable form, before we publish the edited article. This *Accepted Manuscript* will be replaced by the edited, formatted and paginated article as soon as this is available.

You can find more information about *Accepted Manuscripts* in the [Information for Authors](#).

Please note that technical editing may introduce minor changes to the text and/or graphics, which may alter content. The journal's standard [Terms & Conditions](#) and the [Ethical guidelines](#) still apply. In no event shall the Royal Society of Chemistry be held responsible for any errors or omissions in this *Accepted Manuscript* or any consequences arising from the use of any information it contains.

Cite this: DOI: 10.1039/c0xx00000x

www.rsc.org/xxxxxx

ARTICLE TYPE

## Radio frequency triggered curcumin delivery from thermo and pH responsive nanoparticles containing gold nanoparticles and its *in vivo* localization studies in orthotopic breast tumor model

N. Sanoj Rejinold<sup>a</sup>, Reju George Thomas<sup>b</sup>, Muthunarayanan Muthiah<sup>c</sup>, K. P. Chennazhi<sup>a</sup>, In-Kyu Park<sup>c\*</sup>,  
5 Yong Yeon Jeong<sup>b</sup>, K. Manzoor<sup>a</sup>, R. Jayakumar<sup>a\*</sup>

Received (in XXX, XXX) XthXXXXXXXXXX 20XX, Accepted Xth XXXXXXXXXXXX 20XX

DOI: 10.1039/b000000x

Non-invasive radiofrequency (RF) electric fields as an energy source for thermal activation of nanoparticles and thereby delivering drugs within cancer cells could be a valuable addition to nano-mediated RF based cancer therapies. Utilizing the high penetration of RF waves, this would be useful for controlled release of encapsulated drug molecules from smart thermo and pH responsive nanoparticles. Herein, we demonstrate that the breast cancer cells could selectively internalize hemocompatible, 170±20 nm sized curcumin encapsulated chitosan-graft-poly (*N*-vinyl caprolactam) nanoparticles containing gold nanoparticles (Au-CRC-TRC-NPs). Au-CRC-TRC-NPs were predominantly accumulated within cytoplasm. After “optimum RF exposure” at 40 watt for 5 minutes, Au-CRC-TRC-NPs absorbed and dissipated energy as heat in the range of 42°C, which is the lower critical solution temperature (LCST) of the chitosan-graft-poly (*N*-vinyl caprolactam), causing controlled curcumin release and inducing apoptosis to 4T1 breast cancer cells. Further, the tumor localization studies on orthotopic breast cancer model revealed that Au-CRC-TRC-NPs could selectively accumulate at the primary and secondary tumors as confirmed by *in vivo* live imaging followed by *ex vivo* tissue imaging and HPLC studies. These preclinical results throw light on their feasibility as a better tumor targetable nanomedicine for RF assisted breast treatment modalities

### Introduction

Breast cancer remains the second most leading cause of women mortality worldwide. In India, it is the same scenario, where 1,000,000 new cases are being reported per year. <sup>1</sup> Though there are number of conventional and advanced treatment regimens, the side effects associated with them are still lethal and unanswered. <sup>2</sup>

Radio frequency (RF) assisted cancer therapy has got tremendous advantages over conventional radiotherapy, as it is completely non-ionizing and non-hazardous. <sup>3</sup> Deep routed cancers can be well treated using RF therapy. There have been various attempts reported to improve RF therapy with special attention in replacing the RF probe with metallic nanoparticles such as gold (Au-NPs) and iron oxide. <sup>4</sup> In the current scenario, major drawback in RF treatment is the invasive mode of treatment. Most of the reported RF assisted cancer therapy has utilized Au-NPs as it is non toxic, compatible with the body and functional. <sup>5</sup> Smart nanomaterials such as thermo and pH-responsive polymers on the other hand, can take advantage of innate tumor micro environment such as acidic pH <sup>6</sup>, poor lymphatic drainage <sup>7</sup>, and leaky vasculature enhancing passive targeting of nanoparticles. <sup>8</sup>

Thermo-responsive polymers such as poly (*N*-vinyl caprolactam) [PNVCL] has been widely used for anti-cancer drug

delivery. <sup>9-16</sup> These polymers can basically act due to their LCST (lower critical solution temperature) for delivering encapsulated drug molecules. The LCST can be modified to attain a specific temperature, usually above the temperature, so that drug molecules could be delivered once it attains this specific LCST. Biopolymers such as chitosan can be conjugated to PNVCL, not only to tune its LCST, but also to impart a pH response. <sup>9</sup>

Naturally occurring polyphenolic phytoconstituent, Curcumin, possess anti-cancer, anti-oxidant, anti-inflammatory, anti-bacterial, wound healing and hepatoprotective activities. <sup>17</sup> The therapeutic efficacy of curcumin is limited due to its poor oral bioavailability <sup>18</sup>, which has been attributed to its poor aqueous solubility and extensive first pass metabolism. Various attempts have been made through encapsulation in polymeric nanoparticles. <sup>19-24</sup> However, no work has been reported in RF assisted curcumin delivery to cancer cells. Thus Combining thermo and pH responsive polymers with Au-NPs would ideally effective for RF assisted curcumin delivery to cancer cells. The whole idea of incorporating Au-NPs is to induce RF assisted heating under optimum RF conditions, which in turn, sensitized by the thermo-responsive polymers allowing the encapsulated curcumin molecules to be eluted out.

The research questions we focused are, (1) how would Au-CRC-TRC-NPs affect the thermo-responsive delivery to breast

cancer cells at optimum RF conditions?; (2) How can these formulation be targeted toward orthotopic breast tumor model?; (3) What would be the tumor localization in a highly metastasized breast tumor model? We hypothesize that, since Au-NPs are RF heatable, the encapsulated curcumin can be released according to the thermo-sensitivity of TRC-NPs via the heat induced from Au-NPs at optimum RF conditions as shown in Fig.1. The Au-CRC-TRC-NPs being smaller in size could easily be targeted to primary as well as metastasized tumors by the EPR (enhanced permeability and retention) effect. Thus, the major goal of our work is to understand the *in vitro* RF response of Au-CRC-TRC-NPs, its *in vitro* efficacy at optimum RF conditions, and finally *in vivo* breast tumor localization capability in detail.

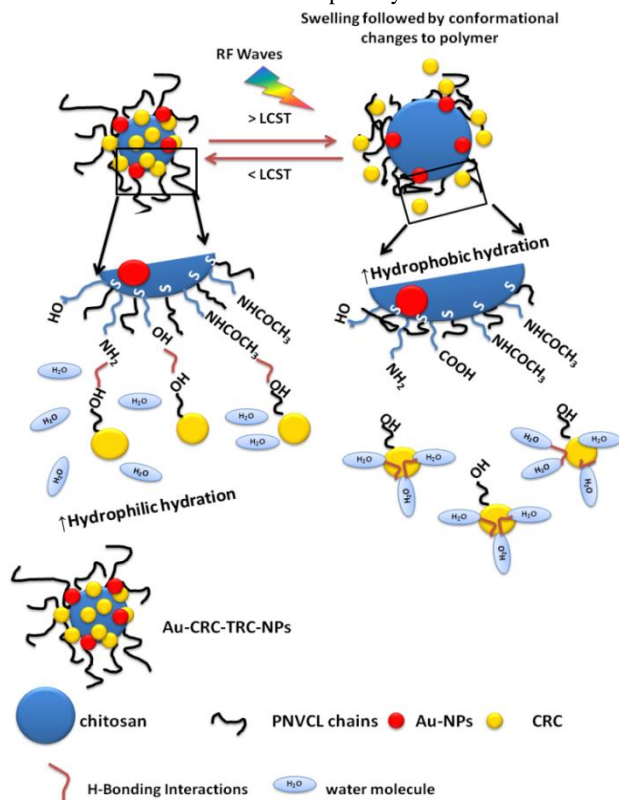


**Fig. 1** The plausible RF assisted thermo-responsive delivery of curcumin to cancer cells above LCST. The increased hydrophobic hydration above LCST and simultaneous RF pulses may enhance thermo-responsive delivery of curcumin to cancer cells

## Experimental

### (a) Materials

Chitosan (Viscosity average molecular weight 20 kDa, Degree of N-deacetylation (75-80%)) was purchased from Koyo chitosan Company, Japan and used as received. *N*-vinylcaprolactam (NVCL) was purchased from Sigma Aldrich and recrystallized from *n*-hexane before use. Azo-bis isobutyronitrile (AIBN), 1-ethyl-3-(3-dimethylaminopropyl) carbodiimide (EDC) and *N*-hydroxy succinimide (NHS), penta sodium tripoly phosphate (TPP) were purchased from Sigma Aldrich, Bangalore, Japan, and used without further purification. Isopropyl alcohol and 3-Mercaptopropionic acid (MPA) were supplied by Aldrich and used as supplied. Curcumin was purchased from Merck, Cochin, India. Acid dextrose citrate, sodium bicarbonate and sodium chloride were purchased from Merck, Cochin for blood compatibility studies. The staining dyes were purchased from

Sigma Aldrich Bangalore. The cell lines were purchased from ATCC, USA.

### (b) Preparation of colloidal gold nanoparticles (Au-NPs)

The gold nanoparticles were prepared according to the existing literature<sup>25</sup> with further modifications for avoiding the ionic concentration in the Au-NPs suspension. 300  $\mu$ L 0.1 M HAuCl<sub>4</sub>·6H<sub>2</sub>O was treated with 10 mL 0.20% starch solution and then 200  $\mu$ L 0.1 M D-glucose was added and allowed the reaction mixture at 50°C. The pH was adjusted with 1% tris buffer solution. A deep wine red coloration after 5 min indicated the formation of 10 nm sized Au-NPs.

### (c) Determination of lower critical solution temperature (LCST)

We analyzed LCST of the systems by UV spectrophotometer (Pharma spec, Japan) starting from a temperature range of 0-45°C and an average of three values were taken as the LCST of the synthesized materials. This was further tested with a digital thermo-meter.

### (d) Preparation of curcumin encapsulated chitosan-graft-PNVCL nanoparticles (CRC-TRC-NPs)

CRC-TRC-NPs were prepared as per our pervious protocol with slight modifications to tune the LCST (42°C).<sup>9</sup> Chitosan-graft-PNVCL was dissolved in acetic acid (1% solution) and the resulting solution was treated with 5mg of ethanolic curcumin (5mg curcumin in 1 mL distilled ethanol), then cross-linked with (sodium tripoly-phosphate) TPP (Sigma-Aldrich) in 1:1 ratio. The resulting CRC-TRC-NPs was centrifuged at 20,000 rpm for 45 min, resuspended and pelletized several times in water until the pH became 7.4.

### (e) Preparation of CRC-TRC-NPs embedded Au-NPs (Au-CRC-TRC-NPs)

Based on trial and error method, the Au concentration was optimized to be 0.54 mg for the 1 mL of CRC-TRC-NPs. The 0.54 mg of Au-NPs were suspended in the 1 mL of CRC-TRC-NPs and incubated at room temperature for about 3 h to complete the reaction. The resulting solution was centrifuged at 20,000 rpm for 5 min and redispersed in distilled water for further studies.

### (f) Preparation of rhodamine-123 labelled-Au-CRC-TRC-NPs Rhod-123-Au-CRC-TRC-NPs

The rhodamine -123 dye is having active -NH<sub>2</sub> which could easily have interaction with -OH and or -COOH functionalities via the hydrogen bonding. The rhodamine-123 encapsulation was done to see the accumulation of nanoparticles in cells by flow cytometry.

The encapsulation of rhodamine-123 was done by adding 40  $\mu$ L dye in 1 mL precursor solution of chitosan-graft-PNVCL in acetic acid. The whole solution was ten stirred for an hour and 1% TPP was added to enable the cross-linking reaction to form final nanosuspension. The Au-NPs directly added to this solution and centrifuged at 20,000 rpm for 5 min to get the final pellet of rhodamine-123 encapsulated nanoparticles. The method was followed for the synthesis of rhodamine encapsulated Au-CRC-TRC-NPs.

**(g) Synthesis of Indocyanin green (ICG) encapsulated Au-TRC-NPs (Au-ICG-TRC-NPs) and Au-CRC-TRC-NPs (Au-ICG/CRC-TRC-NPs)**

ICG was encapsulated by dissolving 0.167 mg/mL ICG in 100% ethanol which was then dissolved in the chitosan-graft-PNVCL/ acetic acid solution. After proper incubation time of 3h, the whole solution was treated with 1% TPP solution followed by 30 minutes stirring for an hour to get the nanosuspension. To this solution, Au-NPs were added and allowed for proper adsorption for 3h. The resulting solution was centrifuged at 20000 rpm for 5 min, and redispersed in distilled water for further studies. The ICG was loaded similarly with Au-CRC-TRC-NPs as described above.

**(h) Leaching studies of ICG from Au-TRC-NPs and Au-CRC-TRC-NPs**

The ICG was detected by IVIS Lumina (Xenogen, CA) with ICG excitation and Emission filters at an exposure value of one second after collecting the supernatants by centrifuging the ICG loaded nanoparticles at 20000 rpm for 5 min. The supernatants were collected at different time periods of day 1, 7, 14 and 30 respectively.

**(i) The loading efficiency (LE) and encapsulation efficiency (EE)**

The LE and EE was determined by centrifuging the drug-loaded nanoparticles at 20,000 rpm for 30 min and separated the supernatant. The supernatant was assayed by UV spectrophotometer (UV-1700 Pharma Spec, Japan) at 428nm by dissolving in ethanol. The calculated LE was 9.2% using the following formula.

$$\% \text{ LE} = \frac{\text{Amount of Drug in NPs}}{\text{Amount of loaded NPs}} \times 100$$

The drug encapsulation efficiency (EE) was defined as the ratio of the mass of the encapsulated drug to the mass of the drug used for nanoparticles preparation using the following equation. The calculated EE was 92%.

$$\% \text{ EE} = \frac{\text{Amount of encapsulated drug}}{\text{Amount of drug used for nanoparticles preparation}} \times 100$$

**(j) *In vitro* quantification of curcumin**

For *in vitro* quantification of curcumin, a standard solution of curcumin in ethanol was prepared by dissolving 5 mg of curcumin in 100 ml ethanol solution. A serial dilution from 0.2 to 2 ml was taken and diluted up to 25 ml and assayed the system at 428 nm using (UV-1700 Pharma Spec, Japan) UV spectrophotometer. The data plotted to get a straight line for the quantification of unknown drug in the nanoparticle.

**(k) Capacitively coupled RF heating of nanoparticle solutions**

**Fig.2** Shows the 13.56 MHz capacitive RF heating system (COMDEL, USA). A 35 x 10 mm petridish petri dish containing 4 mL of aqueous colloidal nanoparticles were positioned on a thin (~0.5 cm) teflon platform (not shown) located mid-plane between two insulated copper electrodes at a spacing of 7.5 cm.

All suspensions were exposed to 40 W of RF generator power resulting in an RF field of 15 kV /m. Reflected RF power was monitored and minimized by impedance matching during RF exposure. The RF exposure system operated at a frequency of 13.56 MHz with an adjustable power output between ~10W to 1000 W. The RF generator/power amplifier (COMDEL, CX1250S/A, cooled RF generator) was connected through a type-N cable to a variable matching network (COMDEL/MATCH PRO CPMX 2500, CODEL INC), which matched the impedance of the power amplifier signal to the water cooled, solenoid antenna. Each sample was exposed to the RF signal at an amplifier setting at 40 W for 300 sec. Temperature change of the solution was measured over time by automatic digital thermometer. The background or unwanted heating was minimized by avoiding the NaOH solution during the Au-NPs synthesis and was replaced with tris-buffer, which had no significant RF heating. The experiments were repeated several times to confirm the accuracy as well the reproducibility under the optimum RF conditions viz 40W and 300 sec RF exposure.

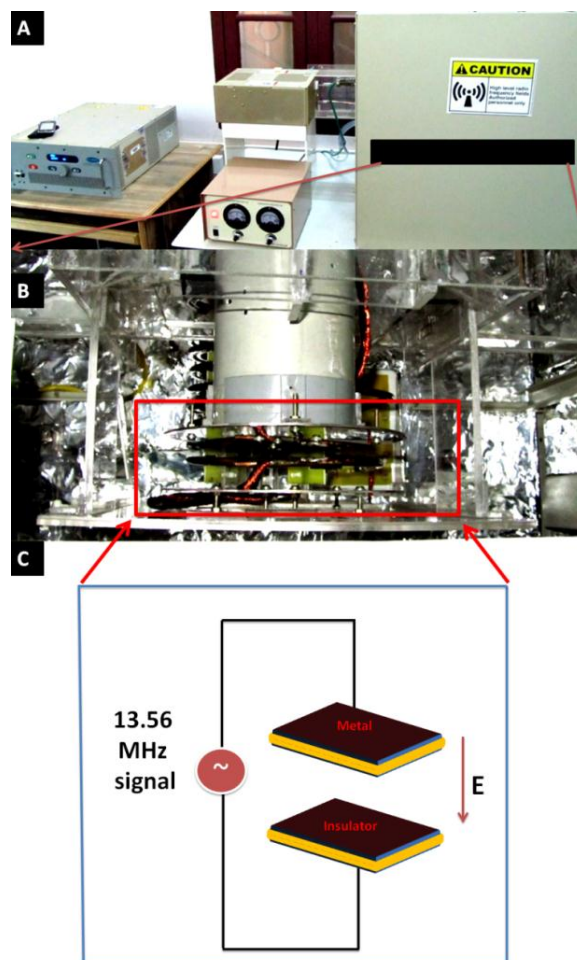


**Fig.2** (A) Prototype capacitive RF heating device. The metal chassis contains high- voltage matching circuits to efficiently produce RF fields between the electrodes. The location of the electrodes within the metal chassis is highlighted by the red rectangle (B) Diagram of the capacitive RF heating system. (C) A 13.56 MHz signal is applied across two metal electrodes (red) that are coated with an insulating Teflon layer (light blue) which produces a high-voltage RF field ( $E = 15 \text{ kV/m}$  at 600 W of RF generator power) over a variable air gap.

### (l) *In vitro* RF assisted curcumin release studies under optimum RF conditions

A known amount of lyophilized Au-CRC-TRC-NPs (50mg) was dispersed in 10 ml deionized water (pH 7.4 adjusted by tris buffer solution) and the solution added into 30 petridishes (500  $\mu$ l each). These were then kept under the RF chamber one by one and RF pulse of 40W for 5 min was given followed by centrifugation of the released curcumin at 15000 rpm for 15 min, dispersed in ethanol to quantify the released amount. The Au-CRC-TRC-NPs have been exposed to the RF pulses at predetermined time intervals via 5 min, 30 min, 1, 3, 6, 9, 12, 24, and 72h respectively to observe the RF assisted curcumin release. The control CRC-TRC-NPs (LCST 42°C) was also analyzed under RF conditions as above. The released curcumin was redissolved in 3 ml ethanol to assay spectrophotometrically at 430 nm. The concentration of released drug was then calculated using standard curve of curcumin in ethanol. The percentage of curcumin released was determined from the following equation

$$\text{Release (\%)} = \frac{\text{Released curcumin from TRC-NPs}}{\text{Total amount of curcumin in TRC-NPs}} \times 100$$

The same protocol was adapted for the RF assisted drug release at 40 W for 5 min with a pH 4.5. The samples were exposed under RF for 5 min at 40W at predetermined time intervals. At each time point, an RF pulse of 40W was given in all the case.

### (m) Cell culture

4T1 (mouse mammary carcinoma cells) and IEC6 (mouse intestinal epithelial cells) were purchased from ATCC, USA. They were maintained in RPMI media supplemented with 10% fetal bovine serum (FBS). The cells were incubated with 5% CO<sub>2</sub>. After reaching confluency, the cells were detached from flask with trypsin-EDTA. The cell suspension was centrifuged at 3000 rpm for 3 min and then re-suspended in the growth medium for further studies.

### (n) Evaluation of cytocompatibility, cellular localization using confocal laser scanning microscopy (CLSM) and flow cytometry

For compatibility experiments, 4T1 and IEC6 cells were seeded on a 96 well plate with a density of 10,000cells/cm<sup>2</sup>. Different concentrations of the samples (0.1, to 1.0 mg/mL) were prepared by diluting with media. For cellular localization studies, the samples of concentration 1mg/mL were treated with 4T1 and IEC6 cells with a seeding density of 5000 cells/well. The cells were harvested after 24h, and washed with PBS twice to remove the non uptaken samples. Since the Rhodamin-123 dye is having innate green fluorescence, we have stained the cells with anti-actin stain (TRITC-conjugated phalloidin dye). Anti-actin dye was stained as per manufacture's protocols. As confocal microscopy gives a better understanding of internalization of particles, this was used to confirm the uptake of our samples by the cells. Since the laser for curcumin excitation (420 nm) was not available with our instrument, Rhodamine labelled samples were used (Rhodamine-123 excitation at 511nm & emission at 534 nm). Acid etched cover slips kept in 24 well plates were

seeded with 4T1 and IEC6 cells respectively, with a seeding density of  $2 \times 10^4$  cells per cover slip and incubated for 24 h for the cells to attach well. After 24 h incubation, the media was removed and the wells were carefully washed with PBS buffer. Then the particle at a concentration of 1mg/ml was added along with the media in triplicate to the wells and incubated for a time period of 24h. After the particular incubation time, anti-actin stain was added as mentioned above and media with sample were removed and the cover slips were processed for confocal microscopy. The processing involved washing the cover slips with PBS and fixing the cells in 3.7% Para Formaldehyde (PFA) followed by a final PBS wash. The cover slips were air dried and mounted on to glass slides with DPX as mountant. The slides were then viewed under the confocal microscope (Leica SP 5 II) to study the internalization of samples. IEC6 and 4T1 cells in its log phase were seeded at a density of 50,000 cells/cm<sup>2</sup> into a 24-well plate. 1mg/mL rhod-Au-CRC-TRC-NPs containing 25  $\mu$ M were made by dilution with the media for this study. After attaining 90% confluency, the cells were washed with PBS buffer, and above mentioned samples were added and incubated at 37°C for 24 h. Intracellular rhod-123-Au-CRC-TRC-NPs fluorescence was analyzed by flowcytometry after excitation with a 488 nm argon laser using FACS Aria II (Beckton and Dickinson, Sanjose, CA). At 530/30 band pass and 502 long pass, fluorescence emission of 515-545 nm from 10,000 cells was collected, amplified and scaled to generate single parameter histogram.

### (o) Anti-cancer efficacy of Au-CRC-TRC-NPs on 4T1 cells under optimum RF conditions

MTT [3-(4, 5-Dimethylthiazole-2-yl)-2, 5-diphenyl tetrazolium] assay for cytotoxic evaluation is a colorimetric test based on the selective ability of viable cells to reduce the tetrazolium component of MTT into purple colored formazan crystals. After reaching 90% confluency, the cells were washed with PBS buffer and 1mg/mL of the samples were added and allowed for particle incubation of 24h. The cells were then washed off with PBS for RF experiments. Since MEM10% contains lots of metallic ions, which could result in unwanted RF heating. To avoid, this we have taken a special media (contains 40% FBS in deionized water for the RF exposure of cells and treated cells at 40W for 5 min. The special FBS media was further replaced with a fresh MEM and incubated further for 48h. The treated and untreated cells were harvested and analyzed for anti-cancer efficacy of Au-CRC-TRC-NPs. Cells in media alone, devoid of nanoparticles acted as negative control and cells treated with Triton X-100 as positive control for a period of 24 h. 5mg of MTT (Sigma) was dissolved in 1 mL of PBS and filter sterilized. 10  $\mu$ L of the MTT solution was further diluted to 100  $\mu$ L with 90  $\mu$ L of serum-free phenol red free medium. The cells were incubated with 100  $\mu$ L of the above solution for 4h to form formazan crystals by mitochondrial dehydrogenases. 100  $\mu$ L of the solubilisation buffer (10% Triton X-100, 0.1N HCl and Isopropyl alcohol) was added in each well and incubated at room temperature for 1h to dissolve the formazan crystals. The optical density of the solution was measured at a wavelength of 570 nm using a Beckmann Coulter Elisa Plate Reader (BioTek Power Wave XS). Triplicate samples were analyzed for each experiment.

**(p) Apoptosis assay by flowcytometry**

## Annexin V-FITC/PI staining

Phosphatidylserine (PS) translocation from the inner to the outer layer of plasma membrane is one of the important earliest apoptotic features. The PS exposure in 4T1 and IEC6 was detected using an Annexin V-FITC/PI Vybrant apoptosis assay kit (Molecular probes, Eugene, OR). The cells were seeded in a 6 well plate with a density of  $1 \times 10^5$  / well. After reaching 90% confluency, the cells were treated with different concentrations of Au-NPs, Au-CRC-TRC-NPs and control CRC-TRC-NPs (1mg/mL) with and without RF exposure as described above. After RF treatment at 40 W for 5 min, the samples were washed off with PBS and a fresh media was added and kept for 48 h at 37°C, cells were harvested by trypsinization and washed with PBS for 5 min followed by centrifugation at 500 g at 4°C. The supernatant was discarded and the pellet resuspended in ice-cold 1X Annexin binding buffer ( $5 \times 10^5$ - $5 \times 10^6$  cells/mL). 2  $\mu$ L of Annexin V-FITC solution and 0.5  $\mu$ L of PI (100 $\mu$ g/mL) were added to 100  $\mu$ L of the cell suspension and mixed gently. The samples were then incubated at room temperature for 15 min in the dark. After incubation, 400  $\mu$ L of ice-cold 1X binding buffer was added, mixed gently, and analyzed by flow cytometry (FACS Aria II ( Beckton and Dickinson, Sanjose, CA). Cells in media alone devoid of any nanoparticles (negative control) and cells treated with control nanoparticles were also analyzed in the same way. Samples were analyzed in triplicates for each experiment.

**(q) Live/dead assay for RF treated and untreated samples**

Live cells are distinguished by the presence of ubiquitous intracellular esterase activity, determined by the enzymatic conversion of the virtually nonfluorescent cell-permeant calcein AM to the intensely fluorescent calcein. The polyanionic dye calcein is well retained within live cells, producing an intense uniform green fluorescence in live cells (ex/em ~495 nm/~515 nm). EthD-1 enters cells with damaged membranes and undergoes a 40-fold enhancement of fluorescence upon binding to nucleic acids, thereby producing a bright red fluorescence in dead cells (ex/em ~495 nm/~635 nm). EthD-1 is excluded by the intact plasma membrane of live cells. The determination of cell viability depends on these physical and biochemical properties of cells. Cytotoxic events that do not affect these cell properties may not be accurately assessed using this method. Background fluorescence levels are inherently low with this assay technique because the dyes are virtually non-fluorescent before interacting with cells. For live/dead assay tests, the cells were seeded on 6 well plates with a seeding density of 50,000 cells. The samples were treated once they reach ~ 80% confluency and assessed for RF experiments under optimum conditions. The RF exposed and un exposed samples were then stained with live/dead assay kit and viewed under fluorescent microscope for the analysis.

**(r) Blood compatibility studies**

**Hemolysis test:** Hemolysis causes damage to red blood cells via the release of iron-containing protein hemoglobin into plasma. To evaluate hemocompatibility of the samples for human use it must be checked for hemolysis analysis. Hemolysis was analyzed based on soret band based absorption of free hemoglobin at 415nm in blood plasma. Fresh blood (10mL) was collected into

1.5mL acid citrate dextrose (ACD) containing tubes. Different concentrations of samples were taken for hemolysis assay. (25, 50, 100, 250, 750 and 1000  $\mu$ g/mL) of each of these samples, 100 $\mu$ L was treated with 1mL of blood and incubated for 2 h at 37°C with shaking in an incubator chamber. PBS and 1% Triton X100 were used as negative and positive controls, respectively. The treated blood was then centrifuged at 4000 rpm for 15min to obtain the plasma. The plasma was collected and 100 $\mu$ L of the plasma was mixed with 1 $\mu$ L of 0.01%  $\text{Na}_2\text{CO}_3$ . The absorbance was measured spectrometrically (UV-1700, Shimadzu) at 380, 415 and 450 nm. The plasma hemoglobin can be calculated using the following equation.

$$\text{Amount of Plasma Hb (mg/dL)} = \{(2A_{415}) - [A_{380} + A_{450}] \times 76.25\}$$

The hemolytic property of nanoparticles was plotted as % hemolysis versus different concentrations of sample. Each concentration was evaluated in triplicate.

$$\text{Hemolysis (\%)} = \frac{\text{Plasma Hb value of Au-CRC-TRC-NPs}}{\text{Total Hb value of blood}} \times 100$$

Plasma coagulation: Interaction of the curcumin nano spheres with the plasma coagulation factors was analyzed by coagulation time measurements. Platelet poor plasma was separated from peripheral blood by centrifugation at 4000 rpm for 15 min at 19°C. 50 $\mu$ L samples of concentrations ranging from 25 to 1000  $\mu$ g/mL were added to 450 $\mu$ L of platelet poor plasma and incubated for 30 min with shaking in an incubator at 37°C. 100 $\mu$ L of prothrombin reagent (Diagnostica stago, France) was added to 50 $\mu$ L treated plasma and the time taken for the plasma to coagulate, i.e., prothrombin time (PT) was measured. In case of activated partial thromboplastin time (aPTT) measurements, 50  $\mu$ L of aPTT activator (Diagnostica stago, France) was added to 50  $\mu$ L of plasma and incubated for 180 sec before the addition of 50 $\mu$ L of 0.025M  $\text{CaCl}_2$ . After  $\text{CaCl}_2$  treatment, the time taken by plasma to coagulate was measured as aPTT. The aPTT value was expressed as aPTT ratio, which can be calculated using the following equation.

$$\text{aPTT ratio} = \frac{\text{aPTT value of Au-CRC-TRC-NPs}}{\text{aPTT value of -ve control}} \times 100$$

Platelet activation and aggregation study : Platelet rich plasma (PRP) was obtained by centrifuging whole blood at 150 g for 10 min at 20 ° C. PRP was diluted ten times using normal saline and the mixture was equilibrated for 30 min at 37°C in a water bath. Diluted PRP (450  $\mu$  L) was treated with the sample (50  $\mu$  L) for 20 min. Saline and 50  $\mu$ M ADP (Sigma, St. Louis, USA) served as negative and positive controls, respectively. Treated PRP (100  $\mu$  L) was incubated with PerCP-Cy5-labeled CD62P and FITC-labeled CD42b (20  $\mu$  L; BD Biosciences, CA, USA) antibodies and incubated for 30 min after which the sample was diluted with PBS and analyzed using flowcytometry. In platelet aggregation analysis, PRP was treated with both graphene systems for 30 min and platelet counting was carried out with a hematology analyzer (Abbott CELLDYN 3700).

**(s) HPLC procedure****Preparation of standard graph of curcumin**

100mg of curcumin was weighed accurately and dissolved in 3 mL of ethanol and added water slowly to make upto 10 mL in a volumetric flask. From this stock solution, aliquots were withdrawn to have concentration range of 2, 4, 6, 8,10  $\mu\text{g/mL}$ . 20 $\mu\text{L}$  of each of these solutions were injected into the HPLC system (LC 2010A HT SHIMADZU). A 75:25 mixture of acetonitrile - 5% acetic acid was used as the mobile phase and a C18 column (5 $\mu\text{m}$ , 3x150mm) was used. At a flow rate of 1mL/min, the retention time of curcumin was  $1\pm 0.2$  min. The detector was set at 429 nm. The peak area under the absorption time curve was noted for each sample and this was plotted against concentration to get the standard graph.

The amount of curcumin detected in plasma and organ tissues were extracted as mentioned above and was quantified by a HPLC method. The sample collected was added with equal volume of distilled ethanol and mixed well to dissolve the curcumin present in it. This was then centrifuged at 5000 rpm for 30 min and the supernatant was filtered using a 22 $\mu\text{m}$  syringe filter. 20  $\mu\text{L}$  of this solution was injected into the HPLC system under the condition mentioned earlier to determine the curcumin concentration.

**HPLC validation curve of curcumin**

From the standard graph plotted (Fig.3), we could see that the regression coefficient value is close to unity indicating linearity for the concentration range selected. As these were reported methods we didn't do the further steps of validation. The standard graph for both the drugs, as shown below is included in the text.

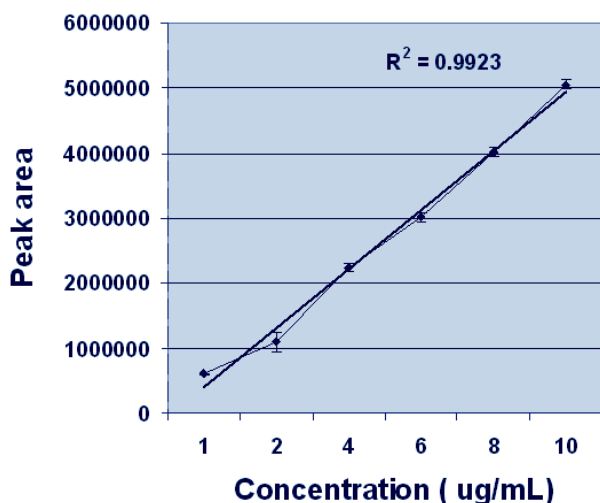


Fig. 3 showing standard graph of curcumin

**(t) Analytical determinations:** FT-IR spectra of materials were carried out using KBr tablets (1% w/w of product in KBr) with a resolution of 4  $\text{cm}^{-1}$  and 100 scans per sample on a Perkin Elmer spectrum RX1 apparatus. The particle size was measured by dynamic light scattering (DLS-ZP /Particle Sizer Nicomp<sup>TM</sup> 380 ZLS) taking the average of 3 measurements. The surface morphology of nanoparticles was analyzed by SEM (JEOLJSM-6490LA) and TEM (Model: JEOL, JEM-2100F). IVIS Lumina (Xenogen, CA) with ICG excitation and Emission filters at an

exposure value of one second. ICP-AES was done at CUSAT, STEC, Kerala India.

**(u) Animal Experiments**

All the animal experiments were performed according to the Ethics Committee of Chonnam National University Medical School and Chonnam National University Hospital, South Korea, Hwasun (CNU IACUC-H-2011-5). Athymic (*nu/nu-ncr*, *Balb/c* mice) with 5-6 weeks old, and 20-25 g weighed nude mice were used for the study. The mice were housed in sterile condition in the laminar flow caging system (Thoren Caging Systems, Inc., Hazleton, PA), and all food, bedding, and water were autoclaved. The 4T1 cells were maintained in RPMI as described earlier. The 4T1 orthotopic tumor model was developed by orthotopic injection of  $1 \times 10^6$  cells/100  $\mu\text{L}$  on the mammary fat pad.<sup>26</sup> The animals were randomized groups of 3 animals received i. v. injections of control ICG and Au-ICG-TRC-NPs and Au-ICG-CRC-TRC-NPs (low and high concentrations viz 5 and 30mg/kg of Au-CRC-TRC-NPs). The imaging was done at different time periods from 5 min to one week. For analyzing the *ex vivo* tissue imaging, the animals were euthanized by cervical dislocation after anesthetizing in a gas anesthesia chamber containing isoflurane at the rate of 2.5% under oxygen supply. The organs such as heart, liver, kidney, brain, stomach, intestine and spleen were collected for imaging after wiping with saline (0.9%). Another set of samples of low and high concentrations via 5 and 30mg/kg of Au-CRC-TRC-NPs and control curcumin were injected to see the tumor localization after one week.

**(v) Quantification of localized curcumin from Au-CRC-TRC-NPs**

The tumor versus organ distribution of curcumin was evaluated by the HPLC as described above.

**(w) Statistics analysis**

The values were expressed in a format of mean  $\pm$  standard deviation (SD). The results obtained were analyzed statistically. A Student's t-test was conducted to determine the significance. A probability level of  $p < 0.05$  was considered to be statistically significant.

**Results**

Different sized Au-NPs have been prepared using starch as coating and D-glucose as reducing agent in presence of tris buffer to get different sized Au-NPs as shown in the Fig.4A-D. Depending on the size the Au-NPs showed different colors starting from wine red to pale violet for 5 to 80 nm sized Au-NPs (Fig.4A-H). This change in color is due to the difference in Surface Plasmon Resonance (SPR) absorption of different sized Au-NPs. The Au-CRC-TR-NPs were prepared by incorporating 10 nm sized Au-NPs (Fig.4I). The exact amount of Au-NPs in Au-CRC-TRC-NPs was found to be 17 ppm as per the ICP-AES.

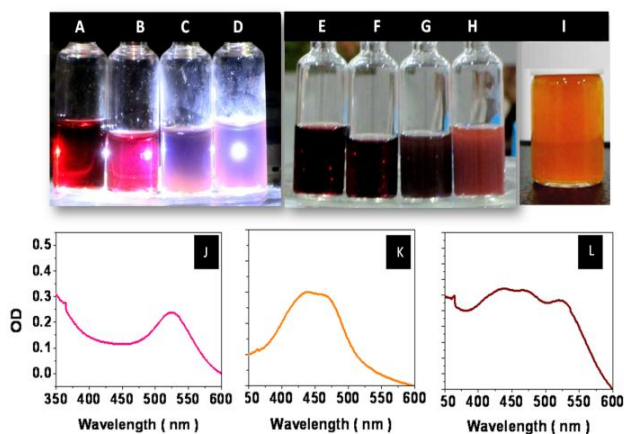


**Fig. 4** (A) (10nm), (B): (20nm), (C): (40 nm) & (D): (80 nm) sized Au-NPs under reflected light and (E-H) normal conditions; stable (I) Au-CRC-TRC-NPs; UV spectra for (J) Au-NPs, (K) Control curcumin loaded TRC-NPs; (L) Au-CRC-TRC-NPs; (M-N) FT-IR and (O) XRD analysis for the samples.

The characteristic peak for Au-NPs at 520 nm (**Fig.4J**) and curcumin's specific peak at 420 nm (**Fig.4L**) were retained in the final nanosuspension of Au-CRC-TRC-NPs ((**Fig.4K**). The exact concentration of Au-NPs presented was validated by ICP and XPS studies. FTIR analysis was done to see the potential interaction between the chemical moieties in the nanoformulation {**Fig.5A (a-d)** and **Fig.5B (a-c)**.

The control Au-NPs showed characteristic peaks of their starch coating at 3430 (-OH stretching vibrations), 2920 (-CH stretching vibration), 1740 (-CO stretching), 1640 (-OH bending vibration), 1462 (-CH deformation), 1375 (-C-CH<sub>3</sub> stretching vibration), 1243 (-OH bending vibration), 1243 (-C-O (acetate), 1100 cm<sup>-1</sup> (-C-O stretching vibration) respectively. (**Fig.5 A(a)**). In Au-TRC-NPs (**Fig.5A(c)**), there was broadening at 3430 and sharpening at 1740 cm<sup>-1</sup> could be due to the combined stretching vibrations from the Au incorporated TRC-NPs. The peaks at 980 cm<sup>-1</sup> also enhanced could be due to the presence of aromatic ring structures of both TRC-NPs and starch coated Au-NPs respectively. The increased -CH stretching vibrations could be attributed to the presence of starch coated Au-NPs on TRC-NPs.

In control ICG (**Fig. 5B(a)**), the sharp and broad peaks at 3400 and 1740 cm<sup>-1</sup> could be attributed to the -NH bending and -CO stretching vibrations respectively. The 1410 cm<sup>-1</sup> peaks representing the SO double bonds in ICG. In Au-CRC-TRC-NPs, there was a sharp peak appeared at 1310 cm<sup>-1</sup> which could be attributed to the linking of strong hydrogen bonding of CRC on Au-TRC-NPs via CRC's OH functionalities. This -OH perturbation in Au-TRC-NPs by the CRC was clear from the -OH widening at 3430 cm<sup>-1</sup> as shown in **Fig.5A(c)**. The Au-CRC/ICG-TRC-NPs showed an extra peak at 1629 cm<sup>-1</sup> could be due to the strong hydrogen bonding interaction of ICG with the Au-CRC-TRC-NPs **Fig.5B(c)**. Apart from this, the peak broadening at 3430 cm<sup>-1</sup> again confirmed the hydrogen bonding within the nanosystems.

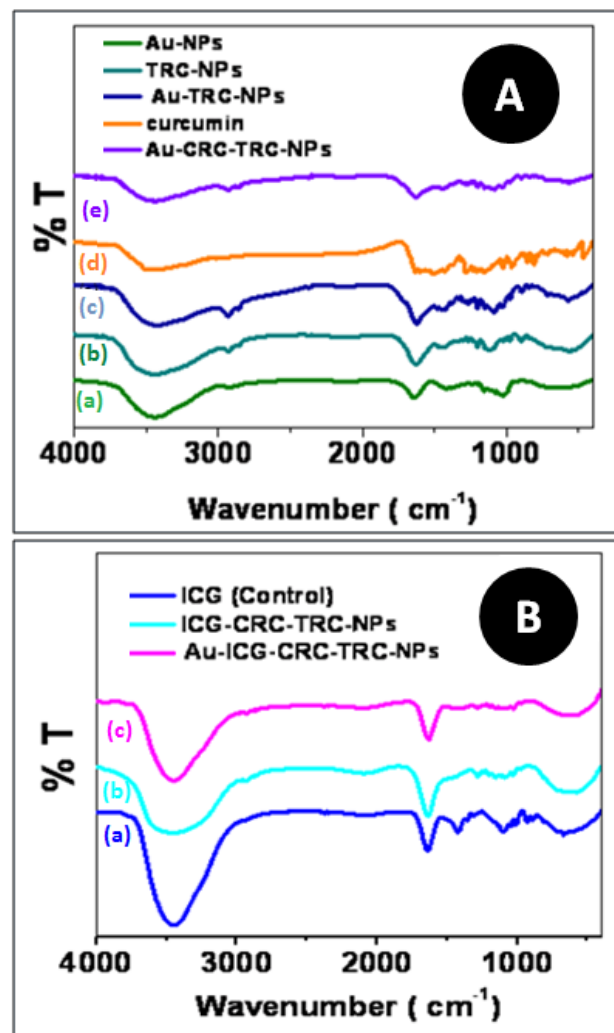


**Fig. 5** FTIR analysis for (A)a: (b) TRC-NPs; (c) Au-TRC-NPs; (d) curcumin; (e) Au-CRCC-TRC-NPs; (B) (a) ICG; 9b) ICG/CRC-TRC-NPs and (c) Au-ICG/CRC-TRC-NPs respectively.

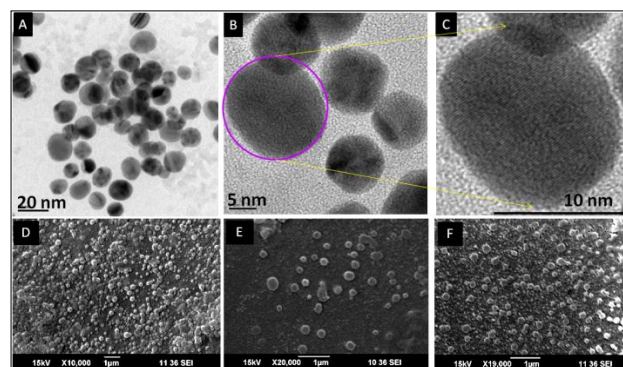


**Fig. 6A-C** HR-TEM images for 10 m sized Au-NPs at different magnifications; SEM analysis for (D) Control Au-CRC-TRC-NPs; (E) Au-ICG/CRC-TRC-NPs; (F) plasma incubated Au-ICG/CRC-TRC-NPs.

Particles size is the key, which can determine circulation half-life and accumulation site in the body<sup>27</sup>. It can also influence the delivery volume and release characteristics for nanodrug carriers<sup>28</sup>. TEM (Fig.6A-C) image shows uniform spherical particle of Au-NPs. The size of Au-CRC-TRC-NPs was  $160\pm 20$  nm (Fig.6D) and Au-ICG-CRC-TRC-NPs had  $170\pm 15$  nm (Fig.6E). The plasma incubated Au-ICG/CRC-TRC-NPs showed almost same particle size of  $170\pm 20$  nm size (Fig.6F). The zeta potential of Au-CRC-TRC-NPs had  $+18\pm 3$  and  $+19\pm 2$  for the Au-ICG-TRC-NPs, respectively.

As shown in the Table 1, the nanosystems have shown particle size in the range of  $< 200$  nm with positive zeta potential.

**Table 1.** Particle size by DLS/SEM, surface charge and PDI analysis for Au-CRC-TRC-NPs, Au-ICG/CRC-TRC-NPs and plasma incubated Au-ICG/CRC-TRC-NPs.

Samples	Particle Size (nm) (DLS)	Particle Size (nm) (SEM)	Zeta Potential (mV)	Poly Dispersity Index (PDI)
Au-CRC-TRC-NPs	$170\pm 15$	$160\pm 20$	$+18\pm 3$	0.256
Au-ICG/CRC-TRC-NPs	$185\pm 5$	$170\pm 15$	$+19\pm 2$	0.267
Au-ICG/CRC-TRC-NPs (Plasma incubated)	$180\pm 15$	$170\pm 20$	$+17\pm 5$	0.232

The cellular localization studies of Au-CRC-TRC-NPs were done on 4T1 and IEC6 cell lines to see their internalization by CLSM Z-stacking followed by flow cytometry. For this, we have utilized the CLSM z-stacking so that exact internalization process can be validated properly. As visualized in the Fig. 7A, B, there was not much difference in internalization between two cell lines, which are of epithelial origin. This was further validated by flow cytometry (Fig. 7C, D).

In general, NaOH used to adjust pH while the preparation of Au-NPs, could lead to an extra heat generation due to the elemental contents of  $\text{Na}^+$  and  $\text{Cl}^-$ . To avoid this situation, we used tris buffer to control the pH of the precursor solutions. The colloidal Au-NPs and Au-CRC-TRC-NPs were found to have RF power as well as concentration dependent heating as shown in Fig.7E & F.

The cells when exposed under RF along with the RPMI media, it can lead to an extra heat due to the elemental contents in media. So we need to replace with some other media while doing RF exposure for 5 min. After RF treatment, the cells can be maintained back in the same RPMI media for further analysis. With different trial, we found that only 40% FBS containing deionized water showed cell survival, which is significantly higher than those treated  $< 40\%$  FBS containing deionized water.

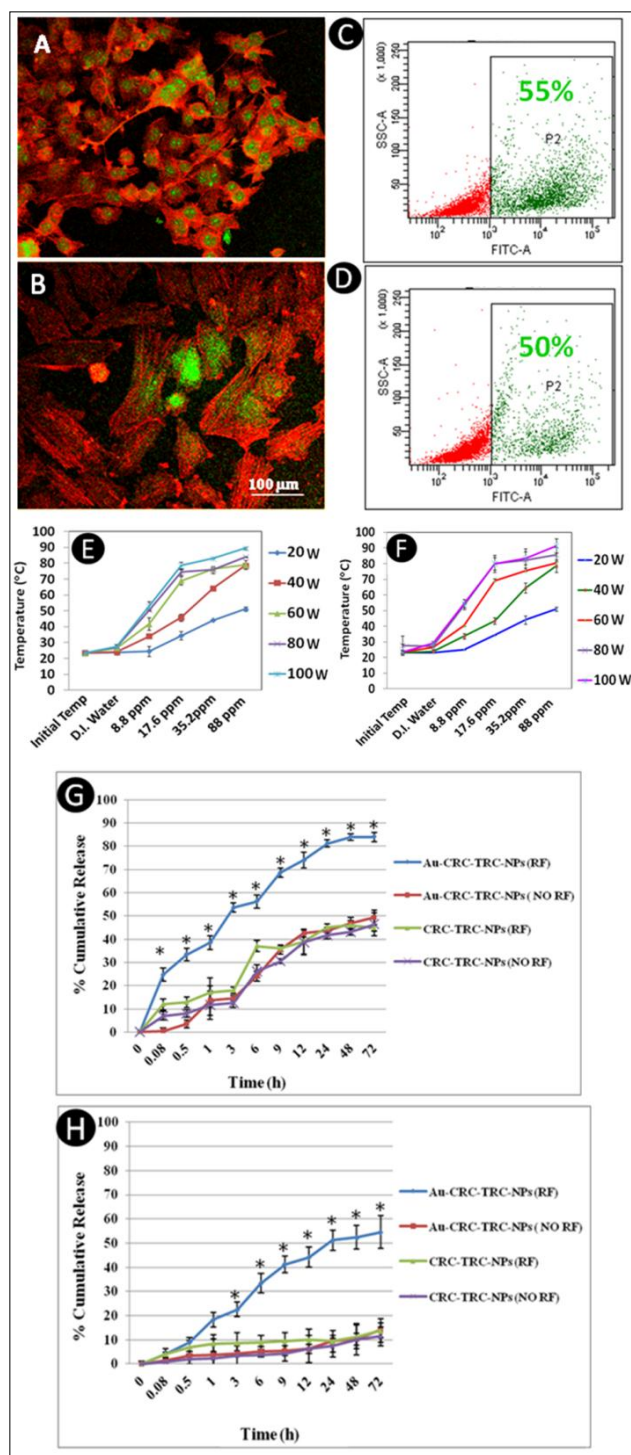


**Fig.7** The cellular localization studies of Au-CRC-TRC-NPs after 24 h on (A) 4T1 and (B) IEC6 cells by confocal and flow cytometry on (C) 4T1 & (D) IEC6 cells. (E) RF assisted heating profile for colloidal Au-NPs; (F) Au-CRC-TRC-NPs with respect to the applied RF power at 5 min; The RF assisted release profile for the colloidal Au-CRC-TRC-NPs & CRC-TRC-NPs at (G) 4.5 & (H) 7.4 pHs . (n=3, \*represents the  $p < 0.05$  level, indicating that the means are significantly different, compared with the control).

For conducting the cellular experiments, we need to replace

media (RPMI) with “specific media”, which does not contain much of ions in it. Thus 40% FBS containing deionized water and checked its RF heating ability for 2 and 5 min, confirming its suitability to replace the cell media, which can avoid unwanted heating. Similarly, we have checked the compatibility of this “special media” on IEC and 4T1 cells by MTT assay after treating the cells with 40% FBS containing deionized water at 40 W for 5 min.

The RF assisted drug release study was conducted in order to assess the effect of RF on the release properties. For this, higher LCST (42°C) was used due to two important factors: 1) cells are more prone for cellular uptake and sensitive for treatment; 2) most of the thermal treatments are being done at above 40°C<sup>29</sup>. As observed in Fig.7G, the RF exposed samples found to have curcumin release significantly higher than the unexposed samples. The release rate was assessed with varying the pH. The RF exposed samples with 4.5 pH had higher release compared to that with pH 7.4 (Fig.7G, Fig.8). However, even without RF, a significant amount of curcumin has been released at acidic pH of 4.5. The effect of Au-NPs on RF assisted curcumin delivery has been confirmed by exposing control CRC-TRC-NPs alone under RF conditions as shown in Fig.7G & H.

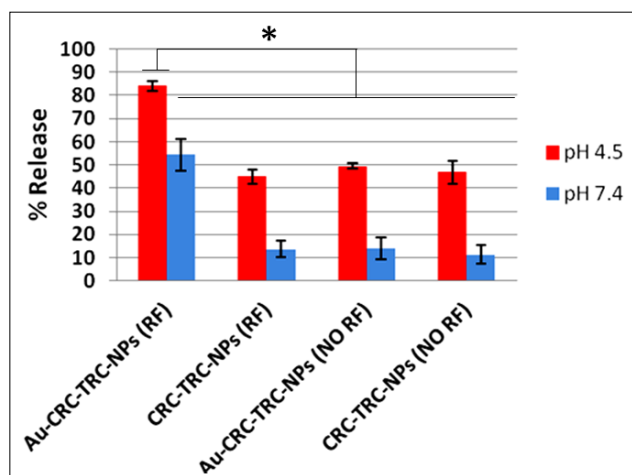


Fig.8 The drug release profile of Au-CRC-TRC-NPs and (B) CRC-TRC-NPs with and without RF exposure at 40W/5min by varying the pHs (7.4 & 4.5) after 24h.

The Au-CRC-TRC-NPs have been tested for its anti-cancer potential against 4T1 cells at optimum RF conditions. IEC6 cells were also tested as control. There was no significant difference in cell death between 4T1 and IEC6 cells. This non specificity could be explained due to the cell line origin, which is same for both 4T1 and IEC6 cells (epithelial cells). However, there was no significant toxicity shown by the treated cells without RF exposure (Fig.9A,B).

Live cells are distinguished by the presence of ubiquitous intracellular esterase activity, determined by the enzymatic conversion of the virtually non fluorescent cell permeant calcein AM to the intensely fluorescent calcein. The polyanionic dye calcein is well retained within live cells, producing an intense uniform green fluorescence in live cells (ex/em ~ 495 nm/ ~ 515 nm). EthD-1 enters cells with damaged membranes and

undergoes a 40-fold enhancement of fluorescence upon binding to nucleic acids, thereby producing a bright red fluorescence in dead cells (ex/em ~495 nm/~635 nm).

MTT results were further validated by live/dead assay. As seen in Fig.9C, the treated 4T1 cells on RF exposure showed a significant red fluorescence compared to the other samples which shows bright green fluorescence indicating the cells were alive.

The apoptotic profile on 4T1 and IEC6 cells were studied after exposing Au-CRC-TRC-NPs treated cells at 40 W RF exposures for 5 min, followed by a pretreatment of 48h prior to the apoptosis detection. There was not much significant difference in apoptosis between IEC6 and 4T1 cell lines (Fig.10). To verify the effect of RF and LCST on apoptosis; we have done the experiments without any RF exposure, which showed no significant apoptosis on both the cell lines (Fig.11).

The RF exposed 4T1 cells showed significant apoptosis compared to without RF exposure. There was ~79±3 % apoptosis on RF exposed 4T1 cells, compared to the unexposed samples. The unexposed samples had ~10±2% of apoptotic cells, which was significantly less compared to the RF exposed one. The 1 mg/mL Au-CRC-TRC-NPs sample was found to be very effective as there was higher apoptosis on 4T1 cells. The 10±2% apoptosis in unexposed cells could be attributed to the pH responsive delivery of curcumin on cells.

It is mandatory to test the hemocompatibility of any drug delivery system prior to the *in vivo* assessments. Therefore the Au-CRC-TRC-NPs with appropriate control samples were tested for blood compatibility as follows.

The interaction of Au-CRC-TRC-NPs with the RBCs can be studied using this test. In general, the interaction of RBCs with the nanoparticles depends on the size, surface charge and functionalities of the nanoparticles. In our study, the different concentrations of Au-CRC-TRC-NPs ranging from 0.01 to 10 mg/mL were exposed with the fresh human blood over a period of 6 h of incubation at room temperature. The % of hemolysis by samples has been tested by measuring the concentration of Hb in plasma obtained after centrifugation. As shown in Fig. 12A, compared to the positive control (Triton X-100 with ~ 100% hemolysis), samples did not show any hemolysis up to 2 mg/mL. These results have been confirmed by taking optical images shown in the Fig. 12B. The Triton treated samples showed a red color due to Hb leakage in to the supernatant unlike the Au-CRC-TRC-NPs treated blood samples, which had shown to have a clear yellowish supernatant with unperturbed RBCs settle down at the bottom of the tubes. SEM analysis was performed to confirm that there is no damage to the RBCs as shown in the Fig.112, D, and showing that the Au-CRC-TRC-NPs even with high concentrations were hemocompatible.

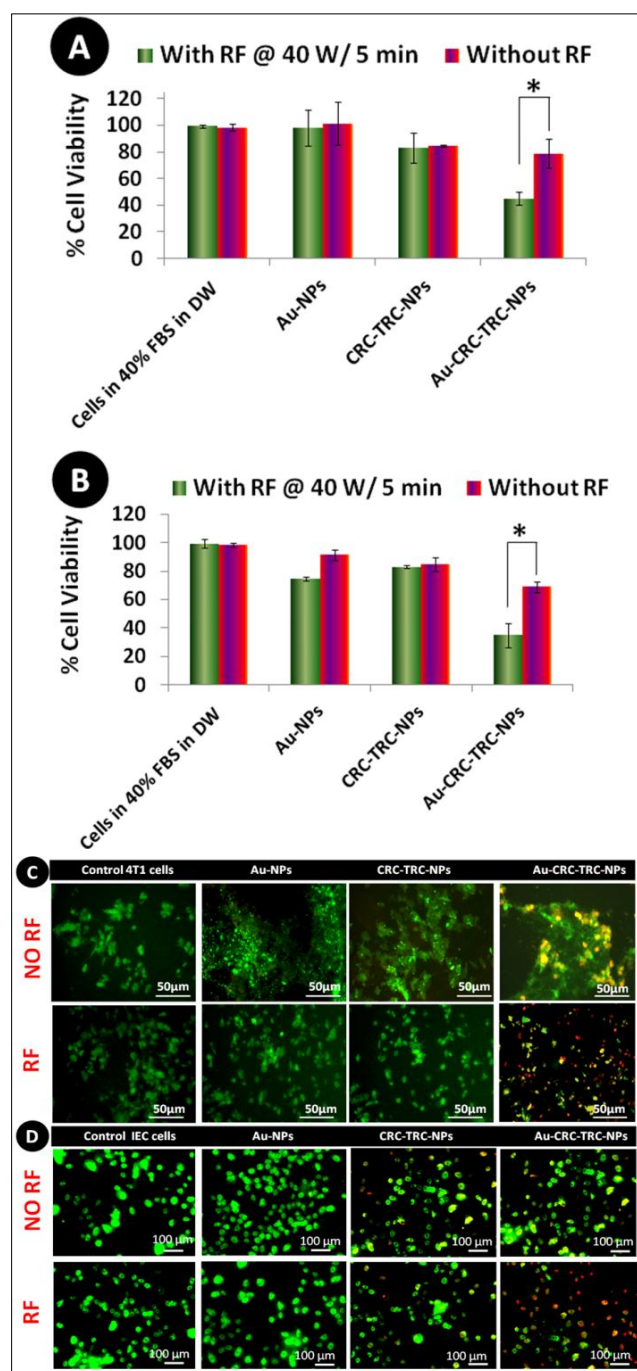


**Fig.9** MTT assay based anti-cancer efficacy of Au-CRC-TRC-NPs on (A) 4T1 and (B) IEC6 cells after 5 min RF exposure followed by 48h incubation; live/dead assay on RF exposed and un exposed treated and un treated (C)4T1 and (D) IEC6 cells (n=3, \*represents p< 0.05 level, indicating that the means are significantly different, compared with the control).

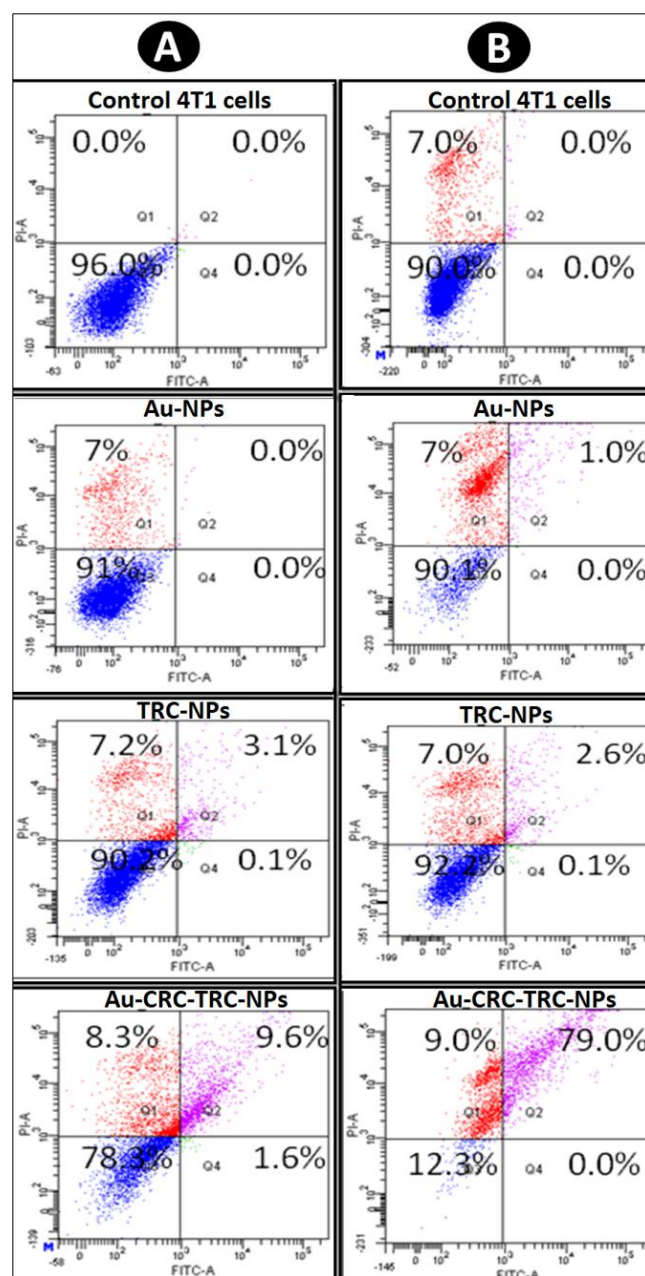


**Fig.10:** Apoptosis profile on 4T1 cells: (A) without and (B) with RF exposure at 40 W/5min.

The basic function of hemostasis is to prevent loss of blood from an injured site and retains the blood fluidity for smooth circulation. Circulating platelets and plasma proteins are the key factors of the hemostatic system. Platelets are having ~ 2  $\mu\text{m}$  size and are more fragile than those of the RBCs. Platelets are responsible for the final step of hemostasis which is thrombus formation. Thee platelet rich plasma (PRP) was incubated with the Au-NPs, CRC controls and Au-CRC-TRC-NPs to assess the platelet activation by monitoring the expression of granular membrane proteins (CD62P) and restricting platelet surface membrane glycoprotein (CD42b) (Glycoprotein Ib). Phosphate-buffered saline (PBS) was used a negative control.

25

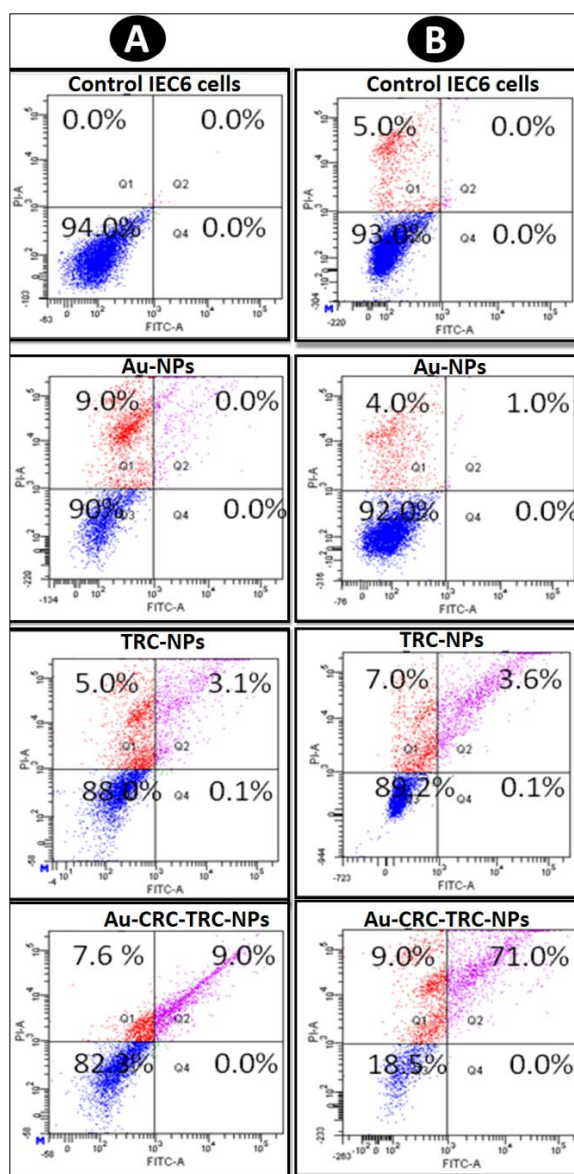


**Fig.11:** Apoptosis profile on IEC6 cells: (A) without and (B) with RF exposure at 40 W/5min.

The flowcytogram showed that PBS-treated platelets indicated a basal activation level of  $\sim 3.4 \pm 3\%$  (**Fig.12E**) and Au-CRC-TRC-NPs (with low and higher concentrations) treated platelets showed only  $\sim 2.3$  and  $\sim 7.4 \pm 1.1\%$  of activation (**Fig. 12F,G**), respectively, suggesting that the Au-CRC-TRC-NPs did not induce platelet activation. This was further confirmed through SEM imaging where the Au-CRC-TRC-NPs-treated platelets (**Fig. 12H, I**) remained discrete and maintained their discoidal shape<sup>30</sup>.

The above results were confirmed by conducting platelet aggregation potential of Au-CRC-TRC-NPs. To maintain the hemostasis, the platelets with other blood components aggregate to form a clot to prevent the excessive blood loss. However, stroke can be expected if the platelet aggregation is excessive in nature.

The platelet count analysis was done to confirm this platelet aggregation by the Au-CRC-TRC-NPs. The PRP treated Au-CRC-TRC-NPs were incubate for 30 min. **Fig. 12K** shows that

while ADP-treated platelets yielded a significant reduction in the count, Au-CRC-TRC-NPs and all the controls viz curcumin, Au-NPs treated platelets maintained a normal count within the range of 50–250 K/ $\mu$ L. This suggested that, as observed in the platelet activation study, neither CRC; Au-NPs nor Au-CRC-TRC-NPs caused platelet aggregation, confirming an effective evidence for their non interaction with the function of platelets.

Mechanism of plasma coagulation consists of intrinsic and extrinsic pathways. These two pathways focused at a major point where factor X gets activated to Xa, activating prothrombin to thrombin and subsequently converts fibrinogen to fibrin. It has been well known that this kind of nanomaterial induced *in vitro* plasma coagulation studies can lay a better platform for the *in vivo* thromogenic potential model. We have assessed the possibility of Au-CRC-TRC-NPs interference with normal coagulation time using prothrombin time (PT) and activated partial thromboplastin time (aPTT) tests. PPP isolated from freshly drawn human whole blood was exposed to different concentrations (0.2–0.4 mg/ mL) of samples and analyzed. PT measurement detects abnormalities of the factors involved in the extrinsic pathway including factors VII, X, V, II, and fibrinogen.

However, it was observed that PT values for all the tested concentrations fall well within the normal range of 12-15 s for all samples, as shown in **Fig. 13A**. Finally we analyzed the effect of samples on intrinsic pathway of plasma coagulation otherwise known as the contact activation pathway, takes place during abnormal physiological conditions such as hyperlipidemic states or bacterial infiltration, which can lead to thrombosis. aPTT registers abnormalities in intrinsic clotting pathway factors including I, II, V, VIII, IX, X, XI, XII, and proteins such as prekallikrein (PK), high-molecular-weight kininogen (HMWK), and fibrinogen.

Precisely, all the above results on hemostasis analysis show that Au-NPs, CRC and Au-CRC-TRC-NPs did not interfere with the normal functioning of platelets or influence the coagulation pathways, and hence may remain non-thrombogenic. Thus Au-CRC-TRC-NPs would be an ideal drug delivery agent for *in vivo* applications and can directly injected on to the blood stream via the intravenous mode of administration, which has more benefits than any other mode of administration, and thus could expect an enhanced therapeutic effect for the bio applications.

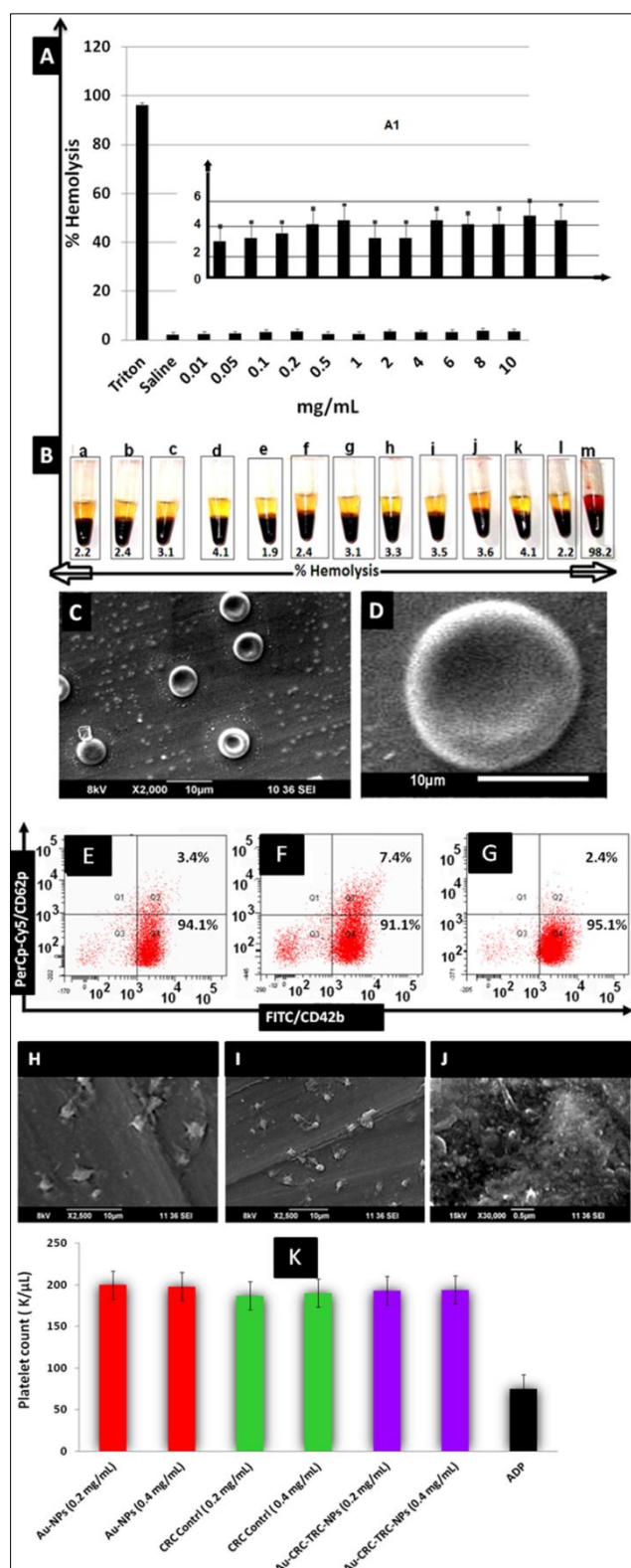


**Fig.12** Hemolysis test on Au-CRC-TRC-NPs.(A) Assessment of whole blood treated Au-CRC-TRC-NPs with varying concentrations from 0.01 to 10 mg/mL. (Inset A1 represents the highlighted portions of the same results from 0-6 % hemolysis for better understanding; (B) Representative optical photographs for the same where a-k shows the concentrations ranging from 0.01 to 10 mg/ml, l is saline, m is triton treated whole blood respectively after 6 h of incubation period. (C) & (D) Shows the low and

higher magnified single image for the high concentrated Au-CRC-TRC-  
 10 NPs treated RBCs without disrupting its innate morphology. Flow  
 Cytometry based platelet activation assessment in (E) PBS; (F) Au-NPs;  
 (G) Au-CRC-TRC-NPs; SEM images of (H) Au-NPs; (I) Au-CRC-TRC-  
 15 NPs treated platelets portraying discrete platelets exhibiting normal  
 morphology whereas the and (J) ADP treated platelets showed activated  
 20 platelets and (K) Platelet count analysis of whole blood treated with  
 varying concentrations of Au-NPs, CRC control and Au-CRC-TRC-NPs,  
 which shows normal platelet counts. (L)Prothrombin (PT) and (M)  
 activated partial thromboplastin time (aPTT) ratio of Au-NPs , CRC  
 and Au-CRC-TRC-NPs (0.2-0.4 mg/mL) treated plasma samples, which  
 shows no significant variation from the normal ranges as shaded in the  
 figure.

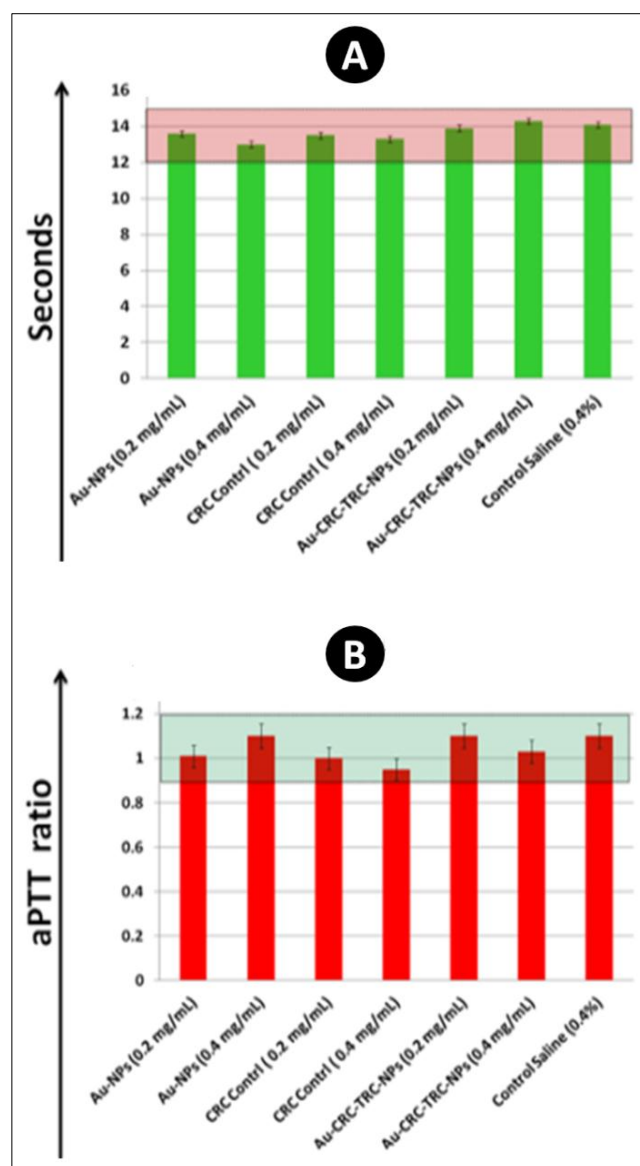


**Fig. 13B** shows that the aPTT ratio variation falls within the normal range of 0.9-1.2 for all the tested concentrations

25

Macrophages play an important role in the phagocytosis of foreign bodies as well as in alerting the rest of the immune system against invaders to elicit innate or adaptive immune response. If the nanoparticles impart toxicity to macrophages,  
 30 there will be significant impairment in the immune resistance capacity of subjects. The Au-CRC-TRC-NPs treated

macrophages did not show any uptake even after 6h as shown in Fig.14.

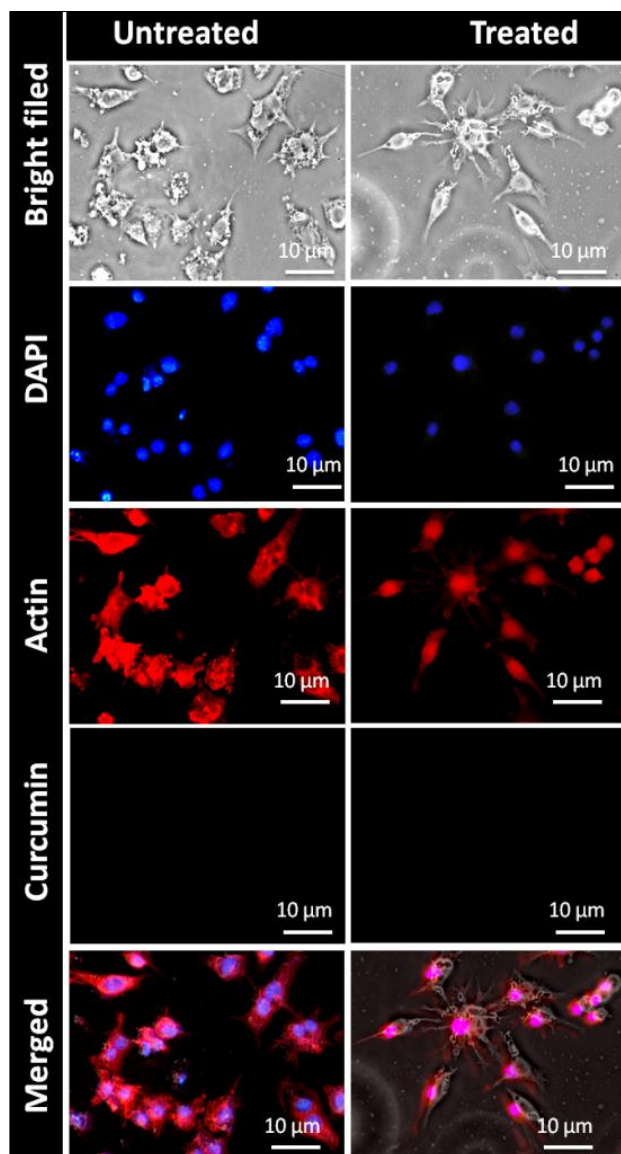


**Fig.14** Macrophage response toward the Au-CRC-TRC-NPs on RAW 246.7 cells after 6 h of incubation period.

4T1 cells are easily transplanted into the mammary gland so that the primary tumor grows in the anatomically correct site. As in human breast cancer, 4T1 metastatic disease develops spontaneously from the primary tumor. Also, the progressive spread of 4T1 metastases to the draining lymph nodes and other organs is very similar to that of human mammary cancer.<sup>31</sup>

As shown in the **Fig.15** the 4T1 tumor models started growing from day 3. There was a sustained growth till day 21. A maximum tumor volume attained was  $\sim 480 \text{ mm}^3$  on 14<sup>th</sup> day.

15

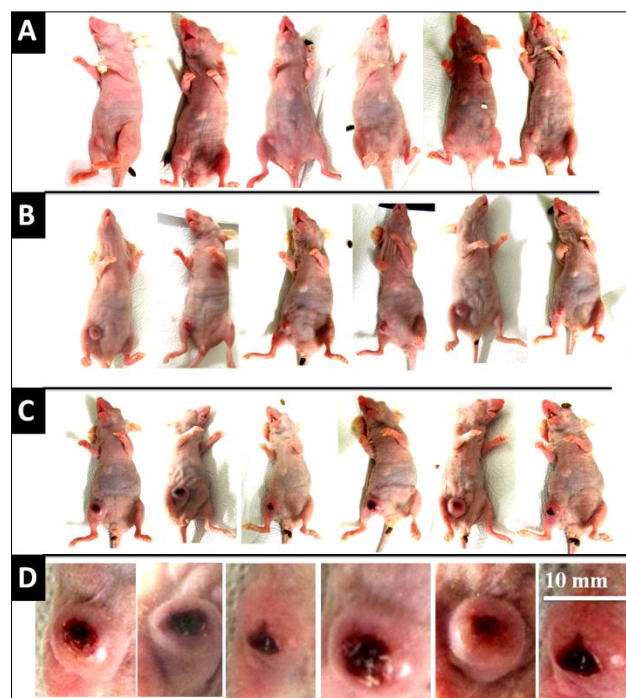


**Fig.15** The growth progress of 4T1 orthotopic breast cancer model after 3<sup>rd</sup>, 5<sup>th</sup>, 7<sup>th</sup> and 14<sup>th</sup> days of tumor cells inoculations.

However the experiments were done on 4T1 tumor with a volume of  $1500 \text{ mm}^3$ . From day 40, the mice showed an extended tumor on the back side of neck (nape) as shown in **Fig.16**.

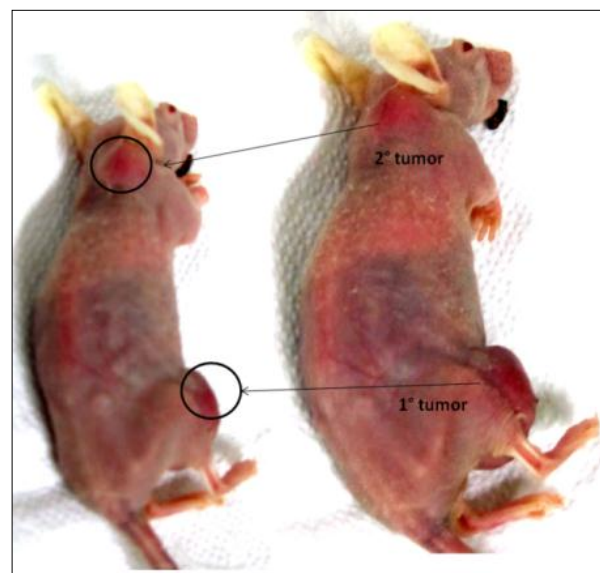


**Fig.16** Metastatic tumor derived from the primary 4T1 breast cancer. A perceptible secondary tumor is visible on the back side of the neck (nape).

The leaching of ICG from Au-ICG-TRC-NPs and Au-ICG/CRC-TRC-NPs were studied by *in vitro* imaging using IVIS Lumina (Xenogen, CA) with ICG excitation and Emission filters at an exposure value of one second. It was necessary to confirm the leaching studies of ICG from the Au-CRC-TRC-NPs prior to

its *in vivo* injection in the tumor mice models. Therefore we have tested the same with different time periods of one day to one month, suggesting that was no significant amount of ICG leaching out from the Au-CRC-TRC-NPs. **Fig.17** shows the leaching studies from Au-ICG-TRC-NPs and Au-IGC/CRC-TRC-NPs.

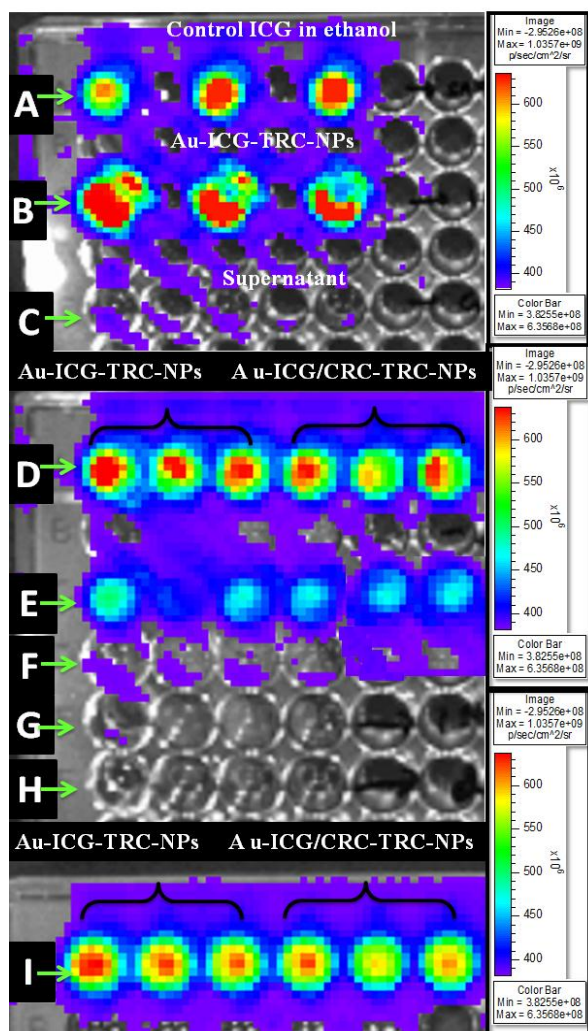


**Fig.17** *In vitro* NIR imaging of ICG encapsulated Au-CRC-TRC-NPs and Au-ICG/CRC-TRC-NPs and the *in vitro* leaching studies of ICG by Xenogen live imaging system. (A) Control ICG dye (0.167 mg/mL); (B) Au-ICG-TRC-NPs (1mg/mL); (C) supernatant; (D) Au-ICG-TRC-NPs and Au-ICG/CRC-TRC-NPs; (E) supernatant after day 1; (F) supernatant after day 7, (G) day 14, (H) after one month and (I) Au-ICG-TRC-NPs and Au-ICG/CRC-TRC-NPs after one month showing intense NIR emission.

The tumor localization of Au-TRC-NPs and the Au-CRC-TRC-NPs was studied by loading with the ICG dye as discussed previously. Au-ICG-TRC-NPs showed tumor localization after 24<sup>th</sup> h as shown in **Fig. 18G**. The samples were compared with the control ICG which got eliminated after 6h (**Fig. 18 D**). The control animal (without any treatment) was also kept for avoiding food fluorescence. In the initial time of 5 min, all the Au-TRC-NPs found to be in the liver. This had been retained till 1 h,

thereafter the Au-TRC-NPs moved toward the intestine with slight intensity toward the tumor area. The same trends had been sustained till 18<sup>th</sup> h, thereafter the intestine intensity got reduced and a maximum tumor accumulation was observed (**Fig. 18F**). On 2nd day, the tumor localization was more clear as most of the Au-TRC-NPs clearly localized on the 4T1 breast tumor model as shown in the **Fig. 18H**. The tumor localization of the Au-TRC-NPs was sustained even up to 7 days (**Fig. 18I-J**) with maximum retention as shown in the higher magnified images (**Fig. 18K-L**).

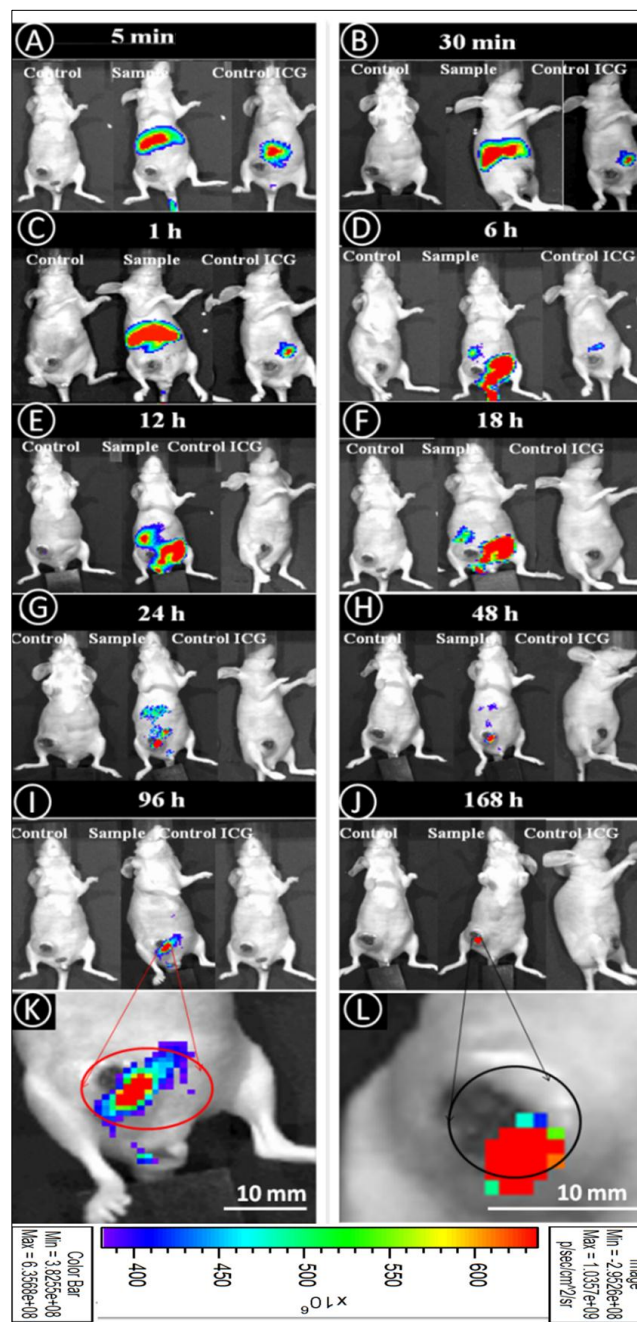


**Fig. 18** The 4T1 breast tumor model showing localization of Au-ICG-TRC-NPs by NIR imaging. (A) 5 min; (B) 30 min; (C) 1h; (D) 6h; (E) 12h; (F) 18h ; (G) 24h; (H) 48h; (I) 96h; (J) 168h imaging after IV administration of Au-TRC-NPs. (K) and (L) represents the higher magnified images for the 96 and 168 h imaging respectively.

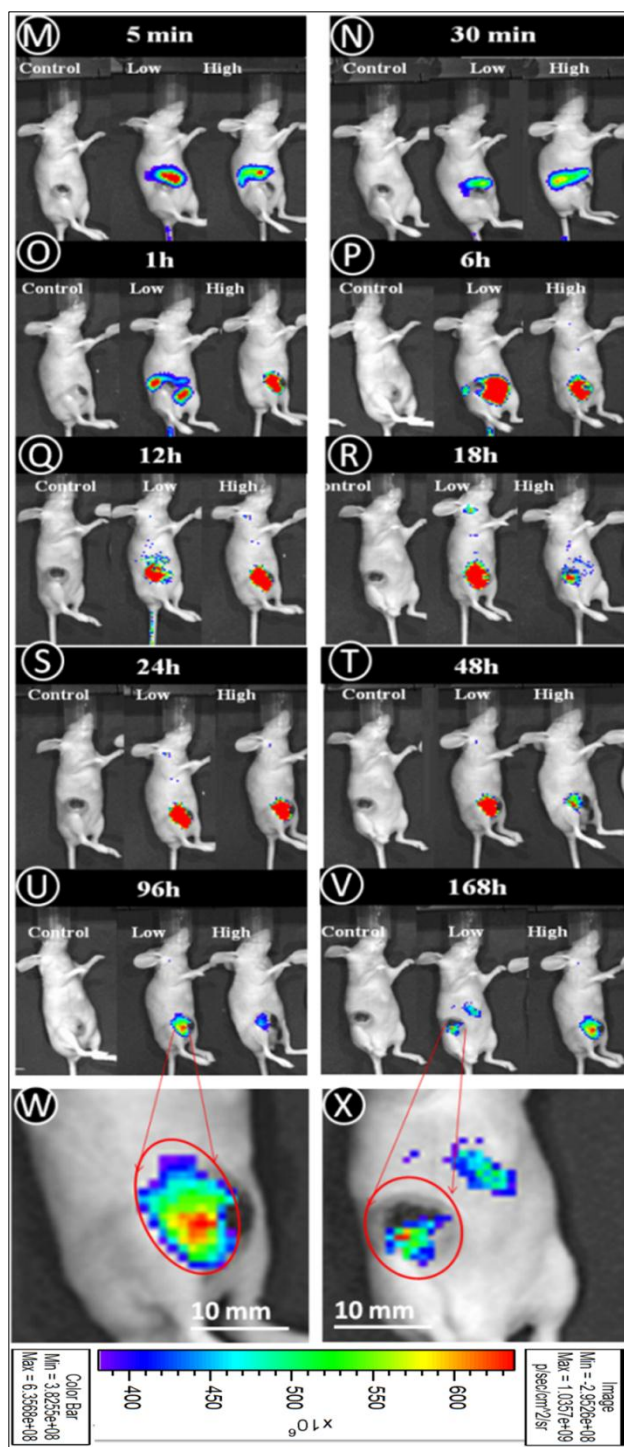


**Fig. 19** Au-ICG-CRC-TRC-NPs localization in tumor model; (M) 5 min; (N) 30 min; (O) 1h; (P) 6h; (Q)12h; (R) 18h ; (S)24h; (T)48h; (U)96h; (V) 168h imaging after IV administration of Au-TRC-NPs; (W) Higher magnified image for Au-ICG/CRC-TRC-NPs injected nude mice after 96 and (X) 168h respectively (low and high concentrations viz 5 and 30mg/kg of Au-CRC-TRC-NPs).

The Au-CRC-TRC-NPs were also analyzed for their tumor accumulation in orthotopic 4T1 orthotopic breast tumor model. The tumor localization was different from the control Au-TRC-NPs. However, the accumulation started from 6th to 18<sup>th</sup> h as shown in **Fig.19 M-X**. On day 1, there was prominent

accumulation with retention of Au-CRC-TRC-NPs at the 15 intestinal region. The accumulation retained same as in 24<sup>th</sup> h, till 72h.

However, there was prominent distribution, both toward tumor and intestinal regions from day 4. 5th day also had same trend. However, on day 7, maximum accumulation was observed in 20 tumor. The experiments were extended upto 2 weeks, confirming the accumulation of Au-CRC-TRC-NPs in tumor for 2 weeks. This high retention of Au-CRC-TRC-NPs could be beneficial for the better regimen for cancer management. There was no reduction in the tumor as the TRC-NPs had the LCST in the 25 range of 42°C. This was expected as encapsulated curcumin could release out only when it attains the LCST at 42°C. Thus it was proved that the TRC-NPs could deliver curcumin only when it attained the maximum LCST range as described.

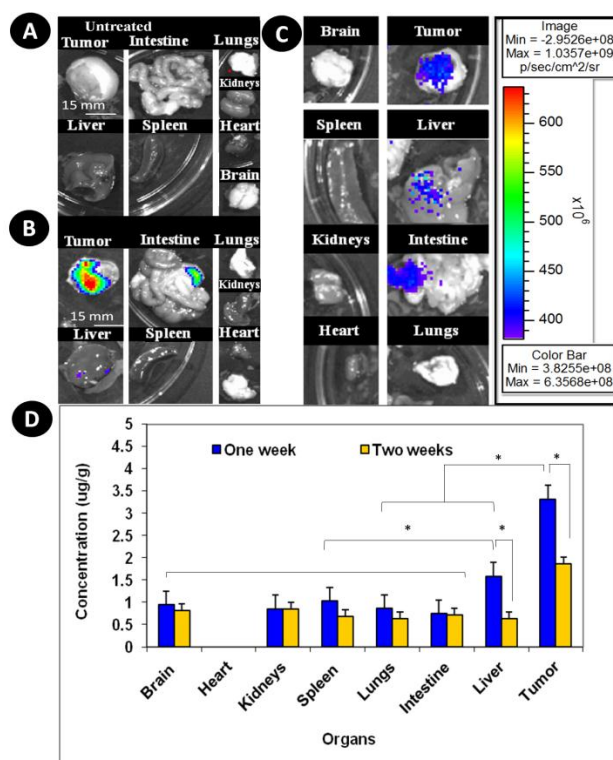


**Fig. 20** *Ex vivo* imaging studies: (A) Untreated organs; (B) Au-ICG-TRC-NPs; (C) Au-ICG/CRC-TRC-NPs injected organs one week after euthanasia. (D) HPLC quantification of curcumin from Au-CRC-TRC-NPs in tumor vs organs after one and two weeks intravenous injection.

35 These results were further validated with *ex vivo* imaging by sacrificing animals on day 7. As shown in **Fig.20A-C**, the tumor had maximum accumulation followed by intestine and liver. The other organs had no significant accumulation.

Further, these results were validated with HPLC quantification 40 as given in **Fig.20D**. The tumor accumulation was significantly higher as 3.6µg/g, whereas other organs did not much amount of curcumin.

As shown in **Fig. 21**, the localization pattern of Au-CRC-TRC-NPs was different in highly metastasized tumor model, compared 45 to the normal orthotopic 4T1 tumor model. During the initial 30 min, the Au-CRC-TRC-NPs were found to be in liver followed

by a drop in liver accumulation over time. Thereafter, the intensity was higher in intestinal regions. By 6<sup>th</sup> and 18<sup>th</sup> h this intensity was found to be enhanced on intestine with negligible intensity on other major organs.

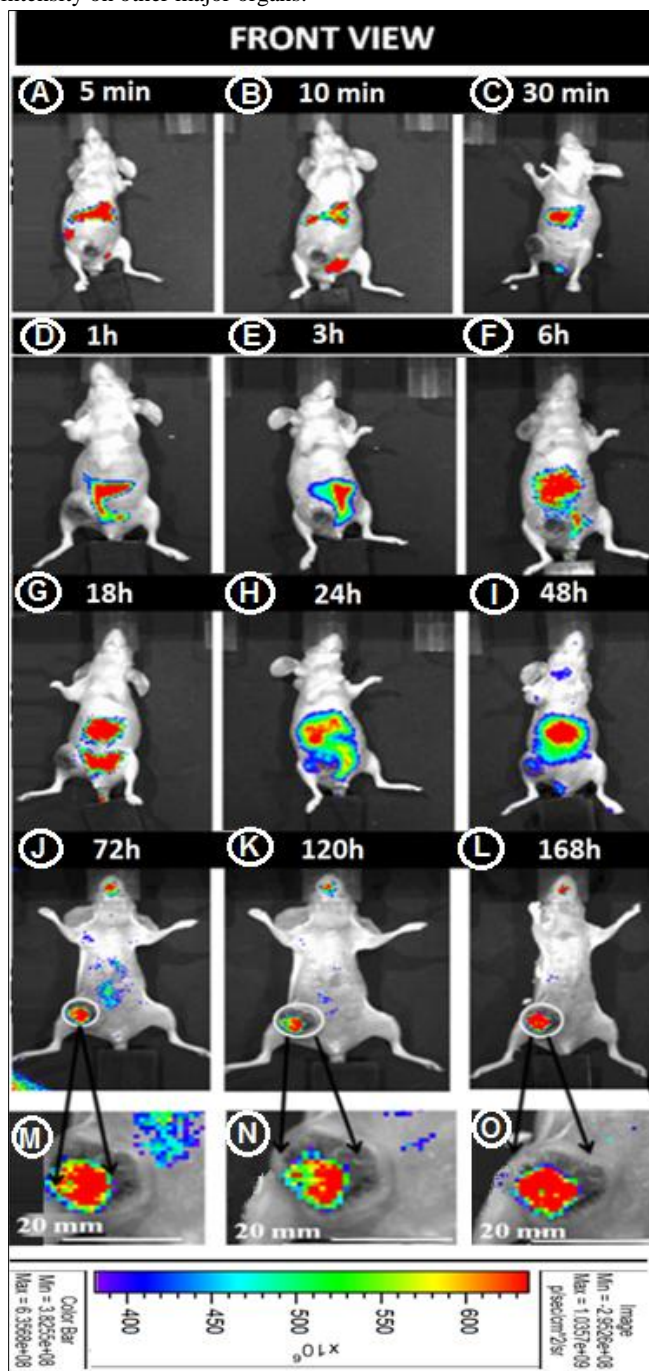


**Fig.21** Metastatic breast cancer localization of Au-CRC-TRC-NPs via (Top view) on nape: Localization at (A) 5, (B) 10 and (C) 30 min; (D) 1, (E) 3, (F) 6h ; (G) 18h, (H) 24 and (I) 48h ;(J)72h, (K)120h and (L) 168h h respectively; (M) represents the higher magnified images for the tumor localization of Au-CRC-TRC-NPs on 72h, (N) 120h and (O) 168h after i.v. administration of ICG loaded Au-CRC-TRC-NPs.

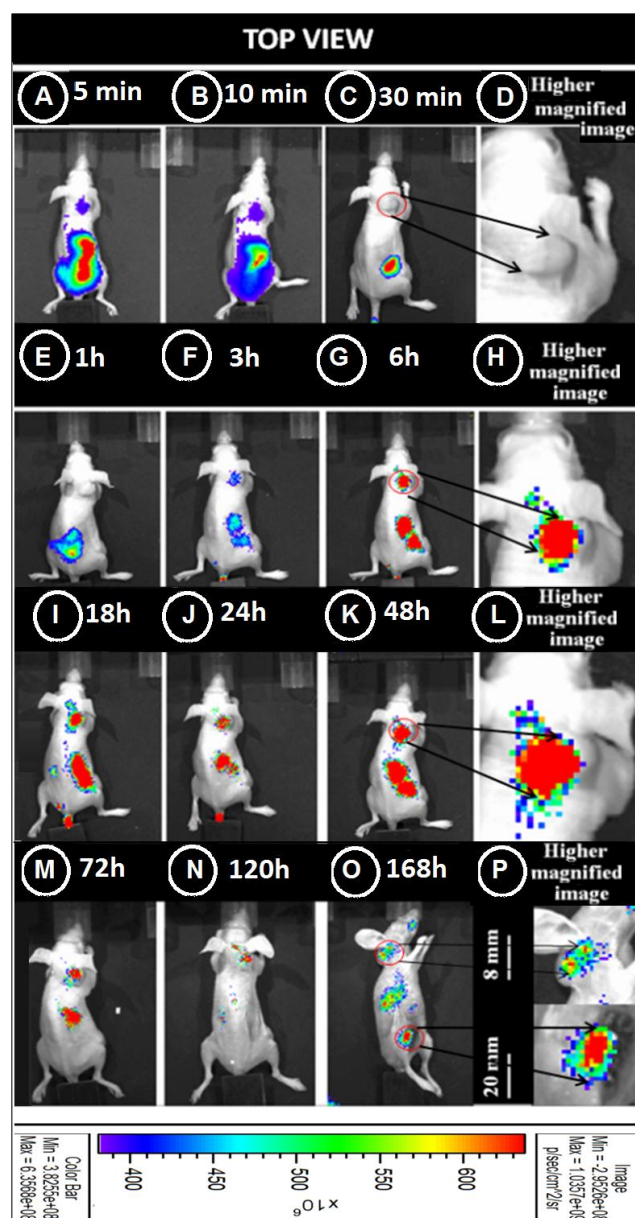


**Fig.22** Metastatic breast cancer localization studies of Au-CRC-TRC-NPs (front view): Localization at (A) 5, (B) 10 and (C) 30 min; (D) 1, (E) 3, (F) 6h ; (G) 18h, (H) 24 and (I) 48h ;(J)72h, (K)120h and (L) 168h h respectively; (M) 72, (N) 120h and (O) 168h (P) its higher magnified image respectively.

However in day 1, the primary tumor showed localization of Au-CRC-TRC-NPs with comparatively higher intensity with maximum localization in the intestinal region. The trend had been found to be same even in day 2. From day 3, there was a clear localization specifically on the tumor (**Fig. 21 (J)**). The localization of Au-CRC-TRC-NPs on 3<sup>rd</sup>, 5<sup>th</sup> and 7<sup>th</sup> day has been shown in magnified images (**Fig. 21 (M, N, & O)**). The top view images shown in the **Fig. 22** clearly demonstrates the accumulation of Au-CRC-TRC-NPs on the secondary tumor developed on the back side of neck (nape). It was very clear that during the initial stages of 5 and 10 min, there was a slight intensity on nape with maximum accumulation in liver. However this trend had been reduced after 30 min to 1 h. 3<sup>rd</sup> h onwards, the

nape intensity was prominent, which further intensified at 6th h as shown in Fig. 22(A-O). Thus it was clear that the nape accumulation of Au-CRC-TRC-NPs sustained for seven days (Fig. 22, P).

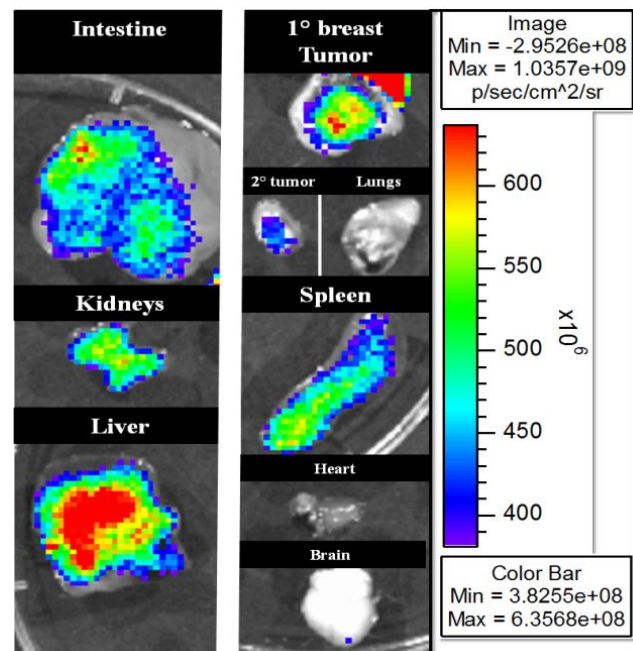


**Fig.23** *Ex-vivo* imaging of Au-ICG/CRC-TRC-NPs in highly metastasized 4T1 breast tumor model one week after i.v injection on primary breast tumor vs secondary tumor developed on nape, and other organs.

Thus it is evident that EPR is the key factor for nanoparticle accumulation in breast tumor. Since 4T1 orthotopic breast tumor model was highly metastasizing, the internal organs could also be accumulated with the Au-CRC-TRC-NPs. Thus *ex vivo* imaging was done to prove this concept. Contrary to the *in vivo* imaging results of 7<sup>th</sup> day, the *ex vivo* imaging showed accumulation in major organs which could be due to less penetrating capability of NIR into the internal organs (Fig.23) whereas, tumors were protruded, enabling an easy detection by NIR imaging. *Ex vivo* studies clearly showed that the 4T1 tumor must have metastasized into liver, spleen, intestine and kidneys. There have been reports for high metastatic trends for 4T1 breast tumor models.<sup>32</sup>

## Discussion

Chitosan-graft-PNVCL has sulphur functionalities in their PNVCL backbone; the incorporated Au-NPs would have a strong binding with them.<sup>33</sup> In addition, the unreacted amines and -OH functionalities could also have strong interaction with the incorporated Au-NPs as shown in Fig.1. The Au-NPs has SPR at 520 nm (Fig.4J), which was evident even after incorporating with CRC-TRC-NPs (Fig.4L), suggesting that there was no perturbation on its SPR. This could be due to the retention of Au-NPs without any changes in its structure within the CRC-TRC-NPs. The possible interaction of Au-NPs thus could be with the sulphur atom present in the chitosan-graft-PNVCL backbone. In

the UV spectrum for Au-CRC-TRC-NPs, the peaks at 430 nm showed the presence of curcumin which again confirmed the balance between two moieties such as Au-NPs and the CRC-TRC-NPs within a single nano-carrier. The optimized concentration of Au-NPs and curcumin for this balanced formulation was 17 ppm and 25  $\mu$ M CRC. There have been reports for the strong interaction of Au-NPs with sulphur links viz thiol groups.<sup>34</sup> Thus there wouldn't be further leaching of Au-NPs from the TRC-NPs. On the other hand, chitosan-graft-PNVCL has strong unreacted amine functionalities which could again increase the hydrogen bonding with Au-NPs and would be more stable. Fig.1 shows the expected interaction of Au-NPs within the nanosystem.

It has already been reported that the permeability of tumor vasculature to nanoparticles is dependent on the tumor type.<sup>35</sup> Some tumors have pore cut off sizes between 400 and 600 nm.<sup>36</sup> Thus ideally the particle size must be below 600 nm for an effective passive delivery towards the tumor sites through EPR effect.

The decrease in zeta potential for CRC-TRC-NPs from control TRC-NPs could be due to the higher loading efficiency of CRC. Similarly after the Au-NPs incorporation, the zeta potential has shifted to a lower value, due to the presence of -OH functionalities from the starch coated Au-NPs. The ICG loaded Au-TRC-NPs had almost the same surface charges as the Au-CRC-TRC-NPs. Since both curcumin as well ICG has similar functional groups viz -OH functionalities, there wouldn't be any changes in their surface charge. The mode of encapsulation of both curcumin as well the ICG were similar. To mimic the exact drug loaded TRC-NPs' nature we have used the hydrophobic ICG for imaging. Thus the synthesized nanosystems have shown particle size within the optimum range for an efficient drug delivery *in vivo*. Since our nanosystems were in the range of <250 nm, a better efficacy would be achieved *in vivo*.

Au-CRC-TRC-NPs didn't undergo macrophage uptake, which could be explained on the basis of the surface charge as well as the chemical compositions of the chitosan-graft-PNVCL backbone. It has been reported that the particle size and surface hydrophilicity play important role to determine the long-term circulation of nanoparticle in the blood stream.<sup>37</sup> The larger particles can be rapidly taken up by the MPS (mono nuclear phagocyte system) cells present in the liver, spleen, and to a lesser extent, in the bone marrow.<sup>38</sup> Hydrophobic surfaces are more prone to opsonization compared to hydrophilic nanoparticles.<sup>39</sup> Surface charge of nanoparticles may also be responsible for suppressing plasma proteins approach. The opsonization existing between the complement proteins involved on the opsonization and the nanoparticles are more favorable to occur on the hydrophobic surfaces than on the hydrophilic ones.<sup>40</sup> Au-CRC-TRC-NPs is expected to possess hydrophilic surface with high affinity to water due to the hydrophilic amines, carboxyl molecules, helping to introduce hydrophilic moieties that camouflage Au-CRC-TRC-NPs and make them invisible to phagocytes.

There have been many reports suggesting that the RF heating of Au-NPs could be due to the "Joule heating". Precisely, the increased resistivity of small sized Au-NPs could impart a higher RF heating due to the increased surface to electron

scattering, as Au-NPs' size is smaller than the mean free path of electrons in it. Similar trend in RF heating of Au-NPs and Au-CRC-TRC-NPs throws light on the fact that, the Au-NPs did not lose its integrity even after incorporating with the CRC-TRC-NPs as proved by UV analysis, where we could see the significant SPR peak in the Au-CRC-TRC-NPs.

Since the Au-TRC-NPs have lot of unreacted amines and acetamide, it could easily swell in the acidic environment enhancing the pH responsive drug release as well. Thus the TRC-NPs could release curcumin not only with the thermal stimulus, but also with the pH. However, there was a significant difference between with RF and without RF in acidic pH environment. It was very clear that even with pH 7.4; with RF, the drug release was very high owing to the thermal stimuli responsive delivery of curcumin from the Au-TRC-NPs. The high release profile of curcumin above LCST could be basically explained by the increased entropic changes along with temperature. Since temperature is directly proportional to entropy (according to Gibb's free energy equation,  $\Delta G = \Delta H - T\Delta S$ ), with increased temperature above LCST, the hydrogen bonding interaction of curcumin with TRC-NPs would be lose and the polymer-polymer interaction would be higher. Since there is a hydrophobic hydration, the released curcumin would have more affinity toward water than the Au-TRC-NPs.

Tager *et al* has already been reported certain thermodynamic conditions for PNVCL solution in the vicinity of the LCST. This could be fulfilled when a favorable conditions such as negative enthalpy  $\Delta H < 0$ ; and a negative entropy  $\Delta S < 0$ ; (2) are attained.<sup>41</sup> The partial Gibbs energy ( $\Delta G$ ), partial enthalpy ( $\Delta H$ ), and partial entropy ( $\Delta S$ ) of mixing of PNVCL solutions were negative over the entire range of composition. Increasing temperature resulted in a decrease in the exothermal character of mixing. Excessive heat capacity values, calculated from the dependencies of enthalpy of mixing on temperature, were positive over the entire composition range. Heat capacity of dilute solutions was measured at 298 K and partial heat capacity of PNVCL at infinite dilution was shown to be positive. The data obtained point out the hydrophilic and hydrophobic hydration of PNVCL in aqueous solutions. Hydrophobic hydration dominates at temperatures close to binodal curve. As a result, the mutual mixing of the polymer with water is decreased and phase separation takes place. This could be the reason why a prominent release was there above LCST with respect to the applied RF power. There are so many controversial results for the hemocompatibility associated with chitosan nanoparticles based on the mode of preparation, solvents used etc. The basic understanding should be given to the sample preparation for hemocompatibility tests. In most of the cases, hemolysis would have happened due to the remnant solvents present in the nanoparticles system, which has to be drained out properly by high centrifugation at 20,000 rpm for 10 min. The resulting pellet should always be redispersed in either saline or PBS to know the actual blood compatibility rather than mixing along with the solvents for blood compatibility assessments. However, these issues could be avoided through proper modification via sulfonation, carboxymethylation and grafting etc. The resulting modified chitosan thus, would be ideal for the *in vivo* applications including drug delivery. Thus the synthesized Au-CRC-TRC-NPs

could be an ideal drug delivery system for *in vivo* applications, where hemocompatibility is an essential factor. Furthermore, maximum dosage of Au-CRC-TRC-NPs could be given intravenously since they are hemocompatible even up to 2mg/mL concentrations.

The tumor localization capability of passively targeted nanoparticle mainly depends on the size, shape and surface charge with chemical compositions.<sup>42</sup> However; there are many parameters which plays crucial role in tumor localization, including the EPR effect. The EPR effect can facilitate an easy accumulation of the injected nanoparticles to a great extent. EPR is the key for many macromolecular and lipid based anti-tumor delivery agents. It has been reported that macromolecule based anticancer agents can substantially accumulate in the tumor<sup>43</sup>, depending on the molecular weight of the anticancer agents. The macromolecules, in particular, those with slight higher molecular weights are well known for their tumor accumulation via the EPR effect.

The EPR effect for the macromolecules has already been observed in many experimental and human solid tumors like Ehrlich carcinoma, mice colon 38 adenocarcinoma, Yoshida AH136B, Wilker 2565 carcinoma and rat tumors, VX-2 carcinoma in rabbits and many human tumors (hepatoma, renal, lung and brain tumors).<sup>44</sup>

In metastasis, the cancer can spread from one organ or part to another non-adjacent organ or part. The new occurrences of disease, thus generated are referred as metastases.<sup>45</sup> Breast cancer is characterized by a distinct metastatic pattern involving the regional lymph nodes, bone marrow, lung and liver. Tumour cell migration and metastasis share many similarities with leukocyte trafficking, which is critically regulated by chemokines and their receptors. 4T1 cancers are well known for its metastatic tumorigenicity similar to the human breast cancers. As shown in **Fig. 16**, primary tumor metastasized perceptibly toward the back side of neck (nape) and developed a tumor with 8.5 mm<sup>3</sup> height.

It is crucial step to see the tumor localization in a metastatic model. As in many human breast cancers; metastasis is a major phenomenon to spread the tumor cells to other unaffected organs and body parts. Since the targeting of our Au-CRC-TRC-NPs was only via the passive mode, it has to be accumulated in the secondary tumors too. In addition, the 4T1 breast tumor can spread toward the lungs, spleen, kidneys, intestine etc.<sup>46</sup> Since EPR is the major key for tumor accumulation of nanoparticles, the Au-CRC-TRC-NPs well accumulated in organs, where angiogenesis was prominent through the metastasis.

## Conclusions

We demonstrated the feasibility of hemocompatible Au-CRC-TRC-NPs as an ideal thermo and pH-responsive RF assisted curcumin delivery agent against breast tumor cells. They also showed potential anti-cancer efficacy on 4T1 tumor cells at optimum RF conditions. In addition, the developed Au-CRC-TRC-NPs were well accumulated in the primary and secondary tumors with maximum retention for seven days. This long term tumor retention of Au-CRC-TRC-NPs was ideal which could replace the daily injection, enabling an enhanced efficacy toward the breast tumors.

## Acknowledgements

Dr. R Jayakumar acknowledges the Department of Biotechnology (DBT), Government of India for supported this work under the Nanosciences & Nanotechnology program (Ref. No. BT/PR10850 /NNT/ 28/ 127/ 2008). Sanoj Rejinold acknowledges the Department of Science and Technology (DST, India) and Ministry of Science, Education and Technology (MEST), South Korea for awarding “Indo Korea-Internship Programme-2013 (Award No: INT/ROK/IKRI-1/2013/6/2/2013”) and Council of Scientific and Industrial Research (CSIR) for the financial support through Senior Research Fellowship (SRF Award No: 9/963 (0017)2K11-EMR-I). The authors are thankful to Mr. Sajin. P. Ravi (SEM studies), Sarath S (confocal Imaging), Sreerexha P R (Flowcytometry), Dr. A. K. K. Unni, Dr. P. Reshmi, Sunil, Sajith, Shantini Narayanan, (Amrita Animal Lab), Dr. T. V. Anil Kumar (SCTIMST Trivandrum), Lee Hwa Jeong, Myeong Ju Moon (Department of Biomedical Science, Research Institute of Medical Sciences, Chonnam National University Medical School, Gwangju 501-746, South Korea) for their technical help.

## Notes and references

- <sup>a</sup> Amrita Centre for Nanosciences and Molecular Medicine, Amrita Institute of Medical Sciences and Research centre, Amrita Vishwa Vidyapeetham University, Kochi-682041, India.
- <sup>b</sup> Department of Radiology, Chonnam National University Hwasun Hospital, Chonnam National University Medical School, Gwangju 501-746, South Korea
- <sup>c</sup> Department of Biomedical Science and BK21 PLUS Center for Creative Biomedical Scientists, Chonnam National University Medical School, Gwangju 501-746, South Korea
- \*Corresponding authors' E-mail ID: (1) [rjayakumar@aims.amrita.edu](mailto:rjayakumar@aims.amrita.edu) & [jayakumar77@yahoo.com](mailto:jayakumar77@yahoo.com) (Prof. R. Jayakumar); Tel: +91 484 2801234 Fax: +91 484 2802020.  
(2) [pik96@chonnam.ac.kr](mailto:pik96@chonnam.ac.kr) (Dr. In-Kyu Park); Tel: +82-61-379-8481; Fax: +82-61-379-8455.
- K. M. Kelly, M. K. Shetty, J. H. T. G. Fregnani, Breast cancer screening and cervical cancer prevention in developing countries: strategies for the future, Breast and Gynecological Cancers, Edited by M. K. Shetty, **2013**, 301-29.
  - S. Borges, H. R. Döppler, P. Storz, *Breast Cancer Res Treatm* **2014**, *144*, 79-91.
  - N. S. Rejinold, R. Ranjusha, A. Balakrishnan, N. Mohammed, R. Jayakumar, *RSC Adv* **2014**, *4*, 5819-25.
  - G. Ferro-Flores, B. E. Ocampo-García, C. L. Santos-Cuevas, E. Morales-Avila, E. Azorín-Vega, *Curr Med. Chem* **2014**, *21*, 124-38.
  - S. Halani, J. Coccagna, E. Chow, K. Hynynen, G. J. Czarnota, Bone Metastases: Cancer Metastasis-Biology and Treatment, Volume 21, 2014, 275-300 edited by V. Vassiliou, E. Chow, D. Kardamakis, Series ISSN 1568-2102, Publisher Springer Netherlands.
  - P. Pellegrini, A. Strambi, C. Zipoli, M. Hägg-Olofsson, M. Buoncervello, S. Linder, A. D. Milito, *Autophagy* **2014**, *10*, 6-15.
  - H. K. Patra, A.P.F. Turner, *Trends Biotechnol*, **2014**, *32*, 21-31.
  - D. Peer, J. M. Karp, S. Hong, O. C. Farokhzad, R. Margalit, R. Langer, *Nat Nano Technol* **2007**, *2*, 751-60.
  - N. S. Rejinold, M. Muthunarayanan, V. V. Divyarani, P. R. Sreerexha, K. P. Chennazhi, S. V. Nair, H. Tamura, R. Jayakumar, *J Colloid Interf Sci* **2011**, *360*, 39-51.
  - N. S. Rejinold, K. P. Chennazhi, S.V. Nair, H. Tamura, R. Jayakumar, *Carbohydr Polym.* **2011**, *83*, 776-86.

- D. Schmaljohann, Thermo- and pH-responsive polymers in drug delivery, *Adv. Drug Deliv Rev* **2006**, *58*, 1655-70.
- N. S. Rejinold, Thejus Baby, K. P. Chennazhi, R. Jayakumar, *Colloids Surfaces B: Biointerf* **2014**, *114*, 209-17.
- T. T. N. Vo, R. Yang, F. Aldabbagh, W. Carroll, M. Meere, Y. Rochev, *J Thermal Sci Eng Appl.* DOI:10.1115/1.4025935.
- B. Y. Swamy, J. H. Chang, H. Ahn, Won-Ki Lee, I. Chung, *Cellulose* **2013**, *20*, 1261-273.
- S. Shah, A. Pa, S. Devi, *J Appl Polym Sci* **2013**, *127*, 4991-99.
- Rao, K. Madhusudana; Rao, K. S. V. Krishna; Sudhakar, P.; Rao, K. Chowdoji; Subha, M. C. *J Appl Pharm Sci* **2013**, *3*, 60-9.
- M. M. Yallapu, B. K. Gupta, M. Jaggi, Subhash C. Chauhan, *J. Colloid Interf. Sci* **2010**, *351*, 19-29.
- P. Anand, A. B. Kunnammakara, R. A. Newman, B. B. Aggarwal, *Mol Pharm* **2007**, *4*, 807-18.
- R. V. Tikekar, Y. Pan, N. Nitin, *Food Res Int.* **2013**, *51*, 370-77.
- Patra, R. Aridi, K. Bouhadir, *Microchimica Acta* **2013**, *180*, 59-64.
- A. L. Palange, D. Di Mascolo, C. Carallo, A. Gnasso, P. Decuzzi, (*In press*) (2014) doi.org/10.1016/j.nano.2014.02.004
- N. M. Khalil, T. C. Frabel do Nascimento, D. M. Casa, L. F. Dalmolin, A. Cristina de attos, I. Hoss, M. A. Romano, R. M. Mainardes, *Colloid Surfac B: Biointerf* **2013**, *101*, 353-60.
- P. Verderio, P. Bonetti, M. Colombo, L. Pandolfi, D. Prosperi, *Biomacromolecules* **2013**, *14*, 672-82.
- R. K. Gangwar, G. B. Tomar, V. A. Dhumale, S. Zinjarde, R. B. Sharma, Suwarna Datar, *J Agric Food Chem* **2013**, *61*, 9632-7.
- E. Christian, H. S. Karsten, Z. Jingdong, C. W. Anna, S. J. Palle, U. Jens, *J Mater Chem* **2009**, *19*, 7839-47.
- S.N. Jiang, T.X. Phan, T.K. Nam, V.H. Nguyen, H.S. Kim, H.S. Bom, H.E. Choy, Y. Hong, J.J. Min. *Mol Ther.* **2010**, *18*, 635-42.
- A. Nagayasu, K. Uchiyama, T. Nishida, Y. Yamagiwa, Y. Kawai, H. Kiwada, *Biochim. Biophys. Acta*, **1996**, *1278*, 29-34.
- A. Ferdous, T. Ishida, M. Shinohara, H. Harashima, H. Kiwada, *Biopharm Drug Dispos.* **1996**, *17*, 145-54.
- J.A. Dickson, B.E. Oswald, *Br J Cancer* **1976**, *34*, 262-71.
- A. Anitha, N. S. Rejinold, J. D. Bumgardner, S. V. Nair, R. Jayakumar, Approaches for functional modification or cross-linking of chitosan. Chitosan-based systems for biopharmaceuticals: delivery, targeting and polymer therapeutics, 107-124, Publisher John Wiley & Sons, Ltd, 2012.
- Pulaski BA, Ostrand-Rosenberg S. Mouse 4T1 breast tumor model. *Curr Protoc Immunol.* 2001 May; Chapter 20: Unit 20.2. Doi: 10.1002/0471142735.im2002s39.
- L. Chen, T.G. Huang, M. Meseck, J. Mandeli, J. Fallon, S. LC Woo, *Mol. Ther.* **2007**, *15*, 2194-202.
- W. Wang, Q. Q. Wei, J. Wang, B. C. Wang, S. H. Zhang, Z. Yuan, *J. Coll. Interf. Sci.* **2013**, *15*, 223-39.
- H. Hannu, *Nat Chem* **2012**, *4*, 443-455.
- F. Yuan, H. A. Salehi, Y. Boucher, U. S. Vasthare, R. F. Tuma, R. K. Jain, *Cancer Res* **1994**, *54*, 4564-68.
- F. Yuan, M. Dellian, D. Fukumura, M. Leunig, D. A. Berk, V. Torchilin, R.K. Jain, *Cancer Res* **1995**, *55*, 3752-56.
- G. Altankov, K. Richau, T. Groth, *Mater.wiss, Werkst.Tech* **2003**, *34*, 1120-8.
- M. Gaumet, A. Vargas, R. Gurny, F. Delie, *Eur J Pharm. Biopharm* **2008**, *69*, 1-9.
- Y. Sheng, Y. Yuan, C. Liu, X. Tao, X. Shan, F. Xu, *J Mater Sci Mater. Med* **2009**, *20*, 1881-91.
- S. Bruno, M. Donatella, C. B. Maria, P. N. Ana, C. M. Maria do, S. Vitor, *Carbohydr Polym* **2011**, *84*, 919-25.
- Q. Kun, T. Ge, L. Peng, C. Qiang, Z. Run, K. Yi-quan, X. Zhi-cheng, Xiao-dan J, *J. Neuroimmunol* **2012**, *242*, 9-15.
- A. Frank, P. Eric, K. M. Linda, C. F. Omid, *Mol Pharm* **2008**, *5*, 505-15.
- J. G. Adam, L. Nate, G. Hamidreza, Enhanced delivery of polymer therapeutics to solid tumors, tailored polymer architectures for pharmaceutical and biomedical applications, Chapter 10, 151-185 Chapter DOI: 10.1021/bk-2013-1135.ch010, ACS Symposium Series, Vol. 1135, ISBN13: 9780841227989eISBN: 9780841227996.

- 
- 44 H. Maeda, J. Wu, T. Sawa, Y. Matsumura, K. Hori, Tumor vascular permeability and the EPR effect in macromolecular therapeutics: a review, *J Control Release* **2000**, *65*, 271-84.
- 45 M. Anja, H. Bernhard, S. Hortensia, G. Nianfeng, C. Daniel, E. B. Matthew, Terri McClanahan, M. Erin, W. Yuan, N. W. Stephan, L. B. Jose, M. Alejandro, V. Emma, Z. Albert, *Nature*. **2001**, *410*, 50-6.
- 46 T. Kai, F. Min, A. Joseph, G. Gary Sahagian, *BMC Cancer* **2008**, *8*, 228-33.